Modelling the Nucleon Axial Form Factor in a Finite Volume

Nathan L. Hall

Supervisors: Prof A. W. Thomas and Dr R. D. Young

Special Research Centre for the
Subatomic Structure of Matter
and
Department of Physics,
University of Adelaide

May 20, 2011

Abstract

Lattice quantum chromodynamics is to date the only way to solve QCD non-perturbatively from first-principles. Although it has enjoyed much success there are still many challenges involved in matching calculated observables with their experimental values. In this thesis we use a chiral model to study the finite volume effects on the axial form factor in order to understand the discrepancy between lattice and experimental results. We also examine the possibility of extra corrections arising from a spin-flip arising through the tensor interaction between neighbouring nucleons on the periodic lattice.

Statement of Originality

This work contains no material which has been accepted for the award of any other degree or diploma in any university or other tertiary institution and, to the best of my knowledge and belief, contains no material previously published or written by another person, except where due reference has been made in the text.

I give consent to this copy of my thesis, when deposited in the University Library, being available for loan and photocopying, subject to the provisions of the Copyright Act 1968.

I also give permission for the digital version of my thesis to be made available on the web, via the University's digital research repository, the Library catalogue, the Australasian Digital Theses Program (ADPT) and also through web search engines, unless permission has been granted by the university to restrict access for a period of time.

Nathan L. Hall

Acknowledgements

I'd firstly like to thank my supervisors Tony Thomas and Ross Young for their constant patience and willingness to help - even when I often turned up unannounced.

I'd also like to thank all my office mates, Adrian, Ben, Daniel and Sam for providing a place to ask those questions I should already have known the answer to and especially to Ben who volunteered to have a look at my thesis. To my house-mates Brad and Tyson, and all the guys in my small group at church, to be able to talk and hang out after uni hours meant I was ready when it was time for work. To Dad, Mum, Jason, Josiah and Becky, thank you for bearing with all the late hours and then for bearing me literally while I had my injured ankle.

And finally I'd like to thank God for his support and guidance throughout the year.

Contents

Chapter 1

Introduction

Understanding the nature of matter and its most fundamental constituents has long been an important part of human endeavour. In today's world there is an ever increasing body of work devoted to this topic. In the realm of subatomic physics, in particular what goes on inside protons and neutrons, the theory which to date best explains what goes on is quantum chromodynamics (QCD).

QCD makes many predictions and these predictions on the whole agree exceptionally well with experiment. Unfortunately, due to the nature of the theory, there are some aspects which cannot be solved using the conventional perturbative techniques. In this low energy region lattice QCD must be used instead.

Lattice QCD is an excellent tool for studying QCD from first principles; however, there are some areas where it is inconsistent with experiment. This thesis will look specifically at the disparity between the lattice and experimental values of the axial form factor - an object which gives information on the structure of the nucleon.

In order for this issue to be clear, a good understanding of the methods lattice QCD uses and how these relate to the continuum case needs to be developed. The second chapter seeks to do this, showing how lattice QCD is obtained from the continuum theory and how the results obtained can be compared with experimental values. The particular case of finding a mass serves as an example. This chapter also includes the details on how the axial form factor was found on the lattice. As well as that there is a discussion on the related observable, the axial radius.

A chiral bag model and its axial form factor will be studied in order to give insight into this problem. It must be pointed out that while this rather basic model fails to replicate precisely the state of affairs on the lattice, the results, as we show, prove remarkably similar.

In chapter 3 we introduce a number of models in order to place this particular chiral model in its correct setting. Chiral symmetry is an important concept in all these models and therefore the chapter begins with a discussion on this symmetry. How it is present and how it is *broken* in nature are also included in this section. The first model reviewed is the MIT bag model, followed immediately by the sigma model. The successes and failures of both are examined before the model that will actually be used - the hedgehog - is described. This chapter is completed with a model known as the cloudy bag model.

Most of the actual calculations that needed to be performed are shown in chapter 4. There is a significant and important amount of background work which needs to be explained and this is done in the first section. The next two sections show the calculations involving the axial form factor and axial radius respectively. The relationship between the two observables are also shown. Results are shown in the chapter that follows, as well as a discussion on what they mean and what can be drawn from them.

In order to include results which more closely resemble the lattice situation, the penultimate chapter includes a (relatively) quick calculation involving the cloudy bag model. The last chapter presents the conclusions of our discussion.

Chapter 2

Lattice QCD

2.1 Overview

It has been known now for a long time that neutrons and protons are not the most fundamental particles of matter but that they are made up of even smaller particles known as quarks and gluons. The interactions between these particles constitute the strong force which binds the nucleus together. Quantum chromodynamics is the gauge theory which governs these interactions [You04]. It makes up part of the Standard Model - the quantum field theory which governs all forces present in Nature except gravity.

One feature unique to QCD is asymptotic freedom: when quarks are close together the force between them is weak - they appear to behave like free particles. However, when they start to be pulled apart the force increases dramatically. A result of this asymptotic freedom is that while we know much about the high energy spectrum of QCD, where perturbative methods work well, the low energy spectrum (i.e. at longer distances) has proven to be much more resistive to solution. In this region, the strong coupling constant α_s becomes large and the perturbative series no longer converge.

To date, the most successful way of solving problems in the low energy limit is lattice QCD (LQCD). In LQCD, the continuum of space-time is replaced by a four-dimensional lattice or "box" with side length usually denoted as L and spacing between points as a. Our infinite path integrals are then replaced with large, but *finite* sums and derivatives by finite differences. In order to compare results from the lattice with experiments, limits need to be taken:

$$\begin{aligned} L &\rightarrow \infty\,, \\ a &\rightarrow 0\,. \end{aligned}$$

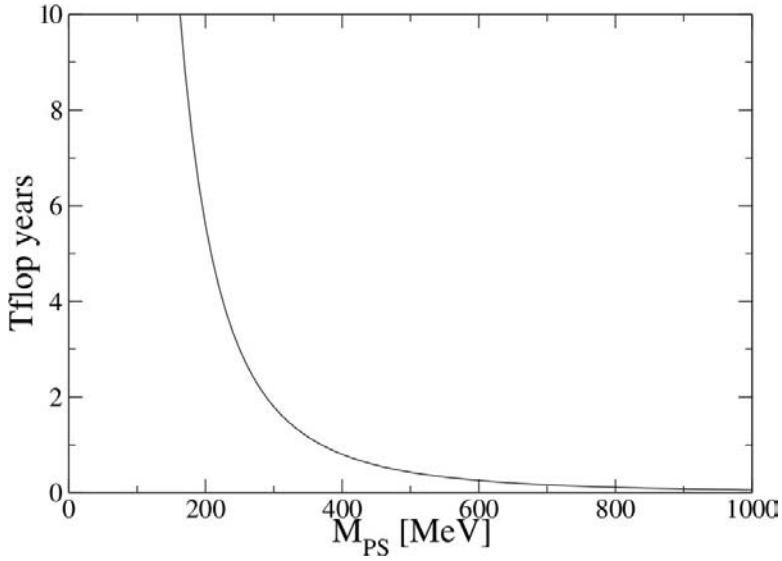

Figure 2.1: Computer time vs pseudoscalar meson mass, for (a) lattice spacing $0.1fm$ (b) lattice volume $(3fm)^3$ (c) 200 configurations and with [Wit02]'s clover action [All05].

However, this process of replacing the continuum theory with a discretised version is not all that straightforward. Computational costs place limits on the size of the box and lattice spacing, not only that but parameters such as the quark and pion masses are restricted to values significantly larger than their experimental ones. A plot taken from [All05] shows the relationship between computational time and mass parameters for a typical lattice configuration. As a result of these restrictions, extrapolation of lattice values is required in order to compare with physical ones. Aside from problems relating to computer power, LQCD must also deal with systematic errors arising from discretisation: by using a finite difference instead of a true derivative in the action, errors of $\mathcal{O}(a)$ are introduced. On top of that, periodicity results in the fermion doubling problem where, for the basic action, there are sixteen fermions on the lattice instead of one!

In spite of these difficulties LQCD has grown into a vast and successful area of research. Modified actions such as the Wilson and staggered[1] actions have dealt with the problem of doubling, while further adjustments have seen $\mathcal{O}(a)$ errors drop to $\mathcal{O}(a^2)$. Although not so common nowadays, the *quenched* approximation - where quark-anti-quark pairs are not included in vacuum -

[1] Although this method also allows from much faster calculations, it suffers from complications involving fermion lattice spacing and extra "tastes" [LTY05].

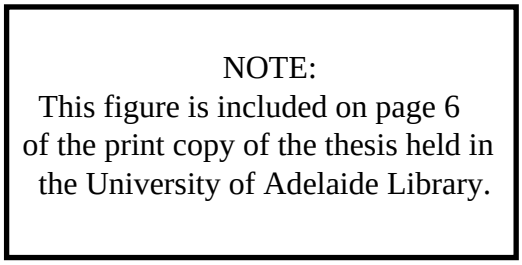

Figure 2.2: Light hadron masses, where π, K and Ξ have been used to set the light quark, strange quark and overall scale [D$^+$08].

was also used and meant that calculations were several orders of magnitude faster [All05], thus going some way to solve the computer power problem.

All these improvements have led to impressive results. Full QCD calculations have now reproduced nucleon masses to within $1-2\%$ [D$^+$08, YT10]; Fig 2.2 shows how close lattice results are to the empirical values for the entire light hadron spectrum. As can be seen below, the pion and kaon decay constants have also been calculated to high levels of precision [D$^+$04]. ("Symanzik-improved" staggered fermions were used here, as opposed to in the above case, where "clover-improved" Wilson fermions were used. However, like Dürr *et al.* the work was done in full QCD.)

Now the story could end there, all we would have to do is wait for the lattice to produce results and show that QCD was the correct theory of strong interactions. Our work, in a sense, would be done. However, this is not the case. There are still some areas where lattice results are considerably different from experiments. Unstable particles and disconnected diagrams still resist the onslaught of LQCD and it may be a while before we can get good results for these values. Another difficult case is the axial form factor.

Lattice results for the axial form factor $G_A(Q^2)$ have consistently predicted results which are flatter than the measured value [AKL$^+$07, OY08, Ale09]. Even the most recent results by Bratt *et al.* [B$^+$10] fail to match those found by pion electroproduction and neutrino scattering methods. A plot from Ref. [Ale09] shows this discrepancy quite clearly. Before we look deeper into this problem though, it is a good idea to look at a brief discussion on general lattice methods so as to have enough background so that when we look at the specific lattice calculations involving the axial form factor we

NOTE:
This figure is included on page 7
of the print copy of the thesis held in
the University of Adelaide Library.

Figure 2.3: A comparison showing the results of unquenched QCD (right-hand side) as opposed to quenched (left-hand side), for a number of different constants [D$^+$04].

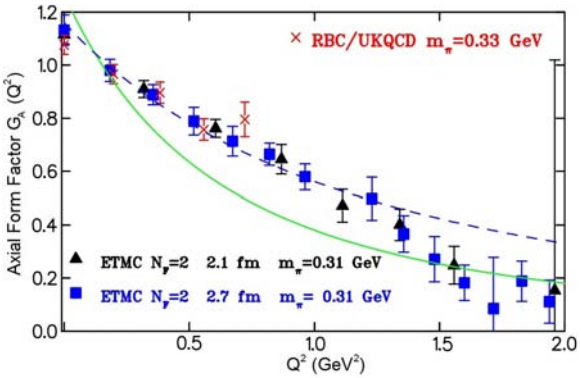

Figure 2.4: Axial form factor vs Q^2. The dashed line is a (dipole) fit to the lattice results, while the solid line represents the experimental results [Ale09].

will be in a better position to understand them. At this point it is important to mention that although we are primarily concerned with the form factor, lattice values of the axial charge - a quantity closely related to the axial form factor - also differs significantly from experimental values [Y+08].

2.2 Lattice Scalar Field Theory

In order to see what a lattice field theory looks like we follow Rothe's example in Ref. [Rot92] of a free scalar field theory. In this case the action is:

$$S = -\frac{1}{2}\int d^4x\phi(x)(\partial_\mu\partial^\mu + M^2)\phi(x). \tag{2.1}$$

To extract information about our theory we need the Green functions and in path integral formulation this gives us,

$$\begin{aligned} G(x,y,...) &= \frac{\int \mathcal{D}\phi\phi(x)\phi(y)...e^{iS[\phi]}}{\int \mathcal{D}\phi e^{iS[\phi]}} && (2.2)\\ &= \langle\phi(x)\phi(y)...\rangle\,. && (2.3)\end{aligned}$$

There is a problem with this equation though: it is extremely difficult to get the right-hand side to converge for numerical simulations [Rot92]. The way round this issue is to make the replacement $x^0 \to -ix_4$ thus transforming our fields into Euclidean space. This is known as a *Wick* rotation. Once all the replacements have been made we get,

$$G(x,y,\ldots) = \langle\phi(x)\phi(y)\ldots\rangle = \frac{\int \mathcal{D}\phi\phi(x)\phi(y)\ldots e^{-S_E[\phi]}}{\int \mathcal{D}\phi e^{-S_E[\phi]}} \tag{2.4}$$

where the Euclidean action is given as,

$$S_E = \frac{1}{2}\int d^4x\phi(x)(-\partial_\mu\partial_\mu + M^2)\phi(x) \tag{2.5}$$

with the μ indices now running from 1 to 4. On a lattice with spacing a the action can be discretised by making the substitutions,

$$\begin{aligned} x_\mu &\to n_\mu a\,, && (2.6)\\ \phi(x) &\to \phi(na)\,, && (2.7)\\ \int d^4x &\to a^4\sum_n\,, && (2.8)\\ \partial_\mu\partial_\mu\phi(x) &\to \frac{1}{a^2}(\partial_\mu\partial_\mu)'\phi(na)\,, && (2.9)\\ \mathcal{D}\phi &\to \prod_n d\phi(na)\,, && (2.10)\end{aligned}$$

where we define the lattice Laplacean as

$$(\partial_\mu \partial_\mu)' \phi(na) = \sum_\mu (\phi(na + \hat{\mu}a) + \phi(na - \hat{\mu}a) - 2\phi(na)) \,. \tag{2.11}$$

With the final exchanges of $\hat{\phi}_n = a\phi(na)$ and $\hat{M} = aM$ our action becomes dimensionless and Eq. (2.4) becomes,

$$\langle \hat{\phi}_n \hat{\phi}_m \ldots \rangle = \frac{\int \prod_l d\hat{\phi}_l \hat{\phi}_n \hat{\phi}_m \ldots e^{-S_E[\hat{\phi}]}}{\int \prod_l d\hat{\phi}_l e^{-S_E[\hat{\phi}]}} \,, \tag{2.12}$$

where $\hat{\mu}$ is a unit vector pointing in the μ direction and

$$S_E = -\frac{1}{2} \sum_{n,\hat{\mu}} \hat{\phi}_n \hat{\phi}_{n+\hat{\mu}} + \frac{1}{2}(8 + \hat{M}^2) \sum_n \hat{\phi}_n \hat{\phi}_n \,. \tag{2.13}$$

In a sense we are done, we have successfully exchanged our continuous path integral over all space-time for a discretised version which works on a finite lattice. Any observable we seek can now be worked out from this new equation. Having said that, as a check, it would be nice to show that by taking the limit $a \to 0$, Eq. (2.12) returns the same value as the continuous one. With this as our aim, we take a look at the two-point correlation function.

The first step to solving this theory is to rewrite the action as,

$$S_E = \frac{1}{2} \sum_{n,m} \hat{\phi}_n K_{nm} \hat{\phi}_m \,, \tag{2.14}$$

where,

$$K_{nm} = -\sum_{\mu>0} [\delta_{n+\hat{\mu},m} + \delta_{n-\hat{\mu},m} - 2\delta_{nm}] + \hat{M}^2 \delta_{nm} \,. \tag{2.15}$$

Beginning with the generating functional[2],

$$Z_0[J] = \int \prod_l d\hat{\phi}_l e^{-S[\hat{\phi}] + \sum_n \hat{J}_n \hat{\phi}_n} \,, \tag{2.16}$$

[2]We dropped the subscript E of the action as we will be in Euclidean space from now on. We have also taken out the summation signs and use the Einstein summation convention instead.

we can diagonalise K_{nm} using orthogonal matices O^T and O to get,

$$Z_0[J] = \int \prod_l d\hat{\phi}_l e^{-\frac{1}{2}\hat{\phi}_n K_{nm}\hat{\phi}_m + J_n\hat{\phi}_n} \tag{2.17}$$

$$= \int \prod_l d\hat{x}_l e^{-\frac{1}{2}\hat{x}_i (O^T)_{in} K_{nm} O_{mj}\hat{x}_j + J_n O_{nk}\hat{x}_k} \tag{2.18}$$

$$= \int \prod_l d\hat{x}_l e^{-\frac{1}{2}D_{ii}(\hat{x}_i)^2} e^{J_n O_{nk}\hat{x}_k} \tag{2.19}$$

where $\hat{\phi}_n = O_{ni}\hat{x}_i$ and $D = O^T K O$ with D being a diagonal matrix. The integral now has a simple Gaussian form, and if we integrate over all the fields we end up with,

$$Z_0[J] = (2\pi)^{\frac{l}{2}} \prod_{i=1}^{l} \frac{1}{D_{ii}} e^{\frac{1}{2}\frac{(J_n O_{ni})^2}{D_{ii}}}\,, \tag{2.20}$$

where l is the number of lattice points. This equation can be manipulated further such that,

$$Z_0[J] = \frac{1}{\sqrt{detK}} e^{\frac{1}{2}J_n K^{-1}_{nm} J_m}\,, \tag{2.21}$$

where we have dropped the $(2\pi)^{\frac{l}{2}}$ term as this "plays no role when computing ensemble averages" [Rot92]. From the Eqs. (2.12) and (2.14) it is not too hard to show that the two-point function is given by,

$$\langle\hat{\phi}_n\hat{\phi}_m\rangle = K^{-1}_{nm}, \tag{2.22}$$

using the relation $KK^{-1} = I$ and the switching to momentum space, we find finally that:

$$K^{-1}_{nm} = \langle\hat{\phi}_n\hat{\phi}_m\rangle = \int_{-\pi}^{\pi} \frac{d^4\hat{k}}{(2\pi)^4} \frac{e^{i\hat{k}\cdot(n-m)}}{4\sum_\mu \sin^2\frac{\hat{k}_\mu}{2} + \hat{M}^2}. \tag{2.23}$$

From this discretised version of the two-point correlation function, we want to be able to produce the *physical* version. To do this we need to reintroduce the lattice spacing a using the substitutions we made earlier and then take the limit $a \to 0$. In this case we have,

$$\langle\phi(x)\phi(y)\rangle = \lim_{a\to 0} \frac{1}{a^2} \int_{-\pi}^{\pi} \frac{d^4\hat{k}}{(2\pi)^4} \frac{e^{i\hat{k}\cdot(\frac{x}{a}-\frac{y}{a})}}{4\sum_\mu \sin^2\frac{\hat{k}_\mu}{2} + a^2M^2}\,, \tag{2.24}$$

then, making the substitution $\hat{k} = ka$ this gives

$$\langle\phi(x)\phi(y)\rangle = \lim_{a\to 0}\frac{1}{a^2}\int_{-\pi/a}^{\pi/a}\frac{d^4k}{(2\pi)^4}a^2\frac{e^{ik\cdot(x-y)}}{4\sum_\mu \frac{4}{a^2}\sin^2\frac{k_\mu a}{2}+M^2}\,. \tag{2.25}$$

Over this interval, the integral will be dominated by the momenta which are small compared to the $\frac{1}{a}$ this means that the sine term in the denominator can be expanded out. After taking the limits we are then left with the familiar expression,

$$\langle\phi(x)\phi(y)\rangle = \int_{-\infty}^{\infty}\frac{d^4k}{(2\pi)^4}\frac{e^{ik\cdot(x-y)}}{k^2+M^2} \tag{2.26}$$

In order to extract a mass, we can use the fact that for large time the correlation function becomes $\sim e^{-M|x-y|}$. As long as the points x and y are known the mass of the state can be found.

To calculate masses on the lattice, we need to move from free fields to interacting theory. Ref. [LMR+05] provides a good discussion of this procedure which we shall follow. To begin an interpolating operator, i.e. creation/annihilation operator, $\mathcal{O}$, needs to be chosen which provides a good overlap with the state of interest. That is, if N is the state being examined, then $\langle 0|\mathcal{O}|N\rangle$ is non-zero and preferably large. The next step involves forming the discrete Fourier transform of the correlation function for a particular point in time,

$$G(t,\vec{k}) = \sum_{\vec{x}}\langle 0|\mathcal{O}(\vec{x},t)\mathcal{O}^\dagger(\vec{0},0)|0\rangle e^{-i\vec{k}\cdot\vec{x}}. \tag{2.27}$$

After that, insert the identity between the two operators and switch to Eu-

clidean space,

$$\begin{aligned}
G(t,\vec{k}) &= \sum_{\vec{x}}\sum_{N}\int \frac{d^3p}{(2\pi)^3 2E(\vec{p})} e^{-i\vec{k}\cdot\vec{x}}\langle 0|\mathcal{O}(\vec{x},t)|N(\vec{p})\rangle\langle N(\vec{p})|\mathcal{O}^\dagger(\vec{0},0)|0\rangle \\
&= \sum_{\vec{x}}\sum_{N}\int \frac{d^3p}{(2\pi)^3 2E(\vec{p})} e^{-i\vec{k}\cdot\vec{x}}\langle 0|e^{i\hat{H}t}e^{-i\hat{P}\cdot\vec{x}}\mathcal{O}(\vec{0},0)e^{-i\hat{H}t}e^{i\hat{P}\cdot\vec{x}}|N(\vec{p})\rangle \\
&\qquad .\langle N(\vec{p})|\mathcal{O}^\dagger(\vec{0},0)|0\rangle \\
&= \sum_{\vec{x}}\sum_{N}\int \frac{d^3p}{(2\pi)^3 2E(\vec{p})} e^{-i\vec{k}\cdot\vec{x}}e^{i\vec{p}\cdot\vec{x}}e^{-iE_N(\vec{p})t}\langle N(\vec{p})|\mathcal{O}(\vec{0},0)|0\rangle \\
&\qquad .\langle N(\vec{p})|\mathcal{O}^\dagger(\vec{0},0)|0\rangle \\
&= \sum_{\vec{x}}\sum_{N}\int \frac{d^3p}{(2\pi)^3 2E(\vec{p})} e^{i(\vec{p}-\vec{k})\cdot\vec{x}}e^{-iE_N(\vec{p})t}|\langle 0|\mathcal{O}|N\rangle|^2 \\
&= \sum_{N}\int \frac{d^3p}{2E(\vec{p})}\delta^{(3)}(\vec{p}-\vec{k})e^{-iE_N(\vec{p})t}|\langle 0|\mathcal{O}|N\rangle|^2 \\
&= \sum_{N}\frac{|\langle 0|\mathcal{O}|N\rangle|^2}{2E_N(\vec{k})}e^{-iE_N(\vec{k})t} \qquad (2.28)
\end{aligned}$$

Performing the Wick rotation $t \to -it$,

$$G(t,\vec{k}) = \sum_{N}\frac{|\langle 0|\mathcal{O}|N\rangle|^2}{2E_N(\vec{k})}e^{-E_N(\vec{k})t} \qquad (2.29)$$

Finally Eq. (2.29) can be approximated by,

$$G(t,\vec{k}) \approx \lambda_0 e^{-M_0 t} + \lambda_1 e^{-M_1 t} \qquad (2.30)$$

where λ_0 and λ_1 are the coupling constants and M_0 and M_1 are the masses of the eigenstates. For large time this becomes,

$$\begin{aligned}
\lambda_0 e^{-M_0 t} + \lambda_1 e^{-M_1 t} &= \lambda_0 e^{-M_0 t}\left(1 + \frac{\lambda_1}{\lambda_0}e^{-(M_1-M_0)t}\right) \\
&\overset{t\to\infty}{\longrightarrow} \lambda_0 e^{-M_0 t} \qquad (2.31)
\end{aligned}$$

where $M_1 > M_0$. So we see that on the lattice the mass of the *lightest* state can be found[3].

Although full LQCD is much more complicated, with fermion fields and interactions both bringing in extra difficulties, the fundamental ideas remain the same. Using this section as a foundation, we can now look at some of the details involved in lattice calculations of the axial form factor.

[3]If $M_0 > M_1$ then the equation would be reversed: with $e^{-M_1 t}$ out the front and $e^{-(M_0-M_1)t}$ inside the brackets

2.3 Axial Form Factor on the Lattice

As it is an important tool in understanding the nucleon, much effort [J$^+$76, GMT83, LDD$^+$94, A$^+$10] has gone into studying the axial form factor. Although Arrington *et al.* were referring specifically to electromagnetic form factors when they expressed them as "... a measurable and physical manifestation of the nature of the nucleons' constituents and the dynamics that binds them together," [ARZ07] such a description would be equally true of the axial form factor. This combination of being measurable and providing such valuable information on the nucleon make it a prime candidate for study on the lattice.

The LHPC collaboration calculated the axial form factor using unquenched QCD. Like Ref. [OY08], and unlike Ref. [Ale09], they use $2+1$ flavours of quarks, with two degenerate, light masses representing the up and down quarks, and a heavier one representing the strange quark. This choice makes their theory much closer to the physical situation [All05].

Using the same lattice spacing $a = 0.124(25)$ fm for each of their ensembles, Bratt *et al.* operated on two different physical volumes: $(2.5 \text{ fm})^3$ and $(3.5 \text{ fm})^3$ respectively. Their pion masses ranged from 293 MeV to 598 MeV, whereas Alexandrou in Ref. [Ale09] performed calculations for m_π as low as 270 MeV, while in Ref. [OY08], 330 MeV.

By using the asqtad action for the sea fermions, Bratt *et al.* were able benefit from the lower computational costs of staggered fermions [You04], as well as enjoying smaller taste (and chiral) symmetry breaking as a result of using fat links [DD]. However there is still some debate over the physical nature of such a description [RT10, Neu04]. For the valence fermions, the domain wall action ensures that chiral symmetry is preserved [H$^+$08]. Alexandrou in Ref. [Ale09] uses a similar mixed action.

In the continuum case the axial form factor is found by placing the Fourier transform of the axial current between any baryon state like so,

$$\begin{aligned} \langle \, \mathrm{B} \, | \vec{j}^{\mu 5}(q) | \, \mathrm{B} \, \rangle &= \langle \, \mathrm{B} \, | \int d^3 r \, e^{i\vec{q}.\vec{r}} \vec{A}^{\mu}(\underline{r}) | \, \mathrm{B} \, \rangle \\ &= \bar{u} \left[G_{\mathrm{A}}(q^2) \gamma^{\mu} \gamma^5 + \frac{i \sigma_{\mu\nu} q_{\nu}}{2m} \gamma^5 G_{\mathrm{T}}(q^2) + q^{\mu} \gamma^5 G_{\mathrm{P}}(q^2) \right] \vec{\tau} u \end{aligned} \tag{2.32}$$

where $\bar{u}$ and u are spinors i.e.,

$$u = \begin{pmatrix} u_p \\ u_n \end{pmatrix} , \tag{2.33}$$

Figure 2.5: Two-point(left) and three-point(right) functions, where A_μ is the axial current [TW].

and $\vec{\tau}$ are the Pauli matrices for isospin. The first and third term are the axial and pseudo-scalar form factors respectively, while the middle term, G_T is the axial tensor term. Although all these form factors are worthy subjects in and of themselves, in this thesis we will only be studying the axial form factor.

In analogy to Eq. (2.32), the operator they ([B$^+$10]) used on the lattice to calculate the matrix element was,

$$\mathcal{O}^{\mu}_{\gamma_5} = \bar{q}(0)\gamma^{\mu}\gamma_5 q(0) \tag{2.34}$$

giving the matrix element for the axial current as,

$$\left\langle k,s|\mathcal{O}^{\mu}_{\gamma_5}|p,r\right\rangle = \bar{u}(k,s)\gamma^{\mu}\gamma_5 u(p,r)\tilde{A}_{10}(t) + \frac{k^{\mu}-p^{\mu}}{2m}\bar{u}(k,s)\gamma_5 u(p,r)\tilde{B}_{10}(t) \tag{2.35}$$

where k and p are the momenta, and s and r the spin of the nucleon. Their form factors are $\tilde{A}_{10}(t)$ and $\tilde{B}_{10}(t)$ the first being the axial and the second, the pseudoscalar form factor with $t = -Q^2$.

To find this matrix element on the lattice, two-point and three-point correlation functions are used, these are shown in Fig. 2.5. Although the principles governing these correlation functions are the same as the one found for the scalar theory, there are extra complications which somewhat hide their similarities. The two-point function in this case looks like [B$^+$10],

$$C^{\text{2pt}}(T,\vec{p}) = \sum_{\vec{x}} e^{-i\vec{p}\cdot\vec{x}} Tr\left(\Gamma_{proj}\langle n(\vec{x},T)\bar{n}(\vec{0},0)\rangle\right) . \tag{2.36}$$

While the expression for the three-point function is,

$$C^{\text{3pt}}(T,T_0,\vec{p},\vec{k}) = \sum_{\vec{x},\vec{y}} e^{-i\vec{k}\cdot\vec{x}+i(\vec{k}-\vec{p})\cdot\vec{y}} Tr\left(\Gamma_{proj}\langle n(\vec{x},T_0)\mathcal{O}(\vec{y},T)\bar{n}(\vec{0},0)\rangle\right) \tag{2.37}$$

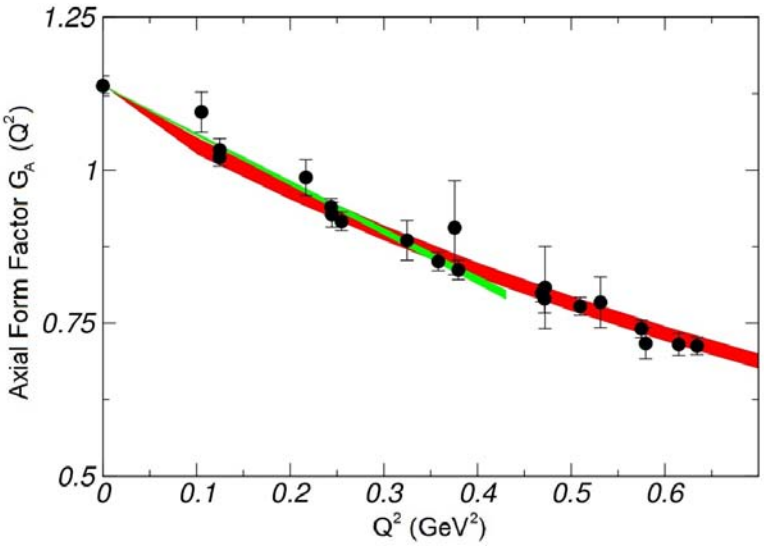

Figure 2.6: Axial form factor of the nucleon versus Q^2 for $m_\pi = 356$ MeV [B$^+$10]. The thick line represents the dipole fit, while the thin line a small-scale expansion fit.

where,

$$\Gamma_{proj} = \frac{1}{2}(1+\gamma_4)\frac{1}{2}(1-i\gamma_3\gamma_5)\,, \tag{2.38}$$

$\bar{p}$ and p are proton creation and annihilation operators, and $\mathcal{O}$ is the axial current mentioned earlier. By dividing the three-point function by two-point functions in the following fashion, [B$^+$10]

$$R(T,T_0) = \frac{C^{3\text{pt}}(T,T_0,\vec{p},\vec{k})}{\sqrt{C^{2\text{pt}}(T,\vec{p})C^{2\text{pt}}(T,\vec{k})}}\sqrt{\frac{C^{2\text{pt}}(T_0-T,\vec{p})C^{2\text{pt}}(T,\vec{k})}{C^{2\text{pt}}(T_0-T,\vec{k})C^{2\text{pt}}(T,\vec{p})}}, \tag{2.39}$$

Bratt *et al.* obtained an expression which, for large enough separation between source and sink, is proportional to the required matrix elements. Fig. 2.6 shows [B$^+$10]'s plot for $G_A(Q^2)$ with pion mass 356 MeV. They include both dipole and small-scale expansion (SSE) fits. However, the SSE depends linearly on Q^2 and so only works for small values of momentum transfer [B$^+$10].

The dipole used was of the form,

$$G_A(Q^2) = g_A\left(\frac{1}{1+\frac{Q^2}{\Lambda^2}}\right)^2, \tag{2.40}$$

with an axial mass $\Lambda = 1.587(29)$ GeV [B$^+$10] which is much greater than the physical values $\Lambda = 1.069(16)$ GeV and 1.026(21) GeV obtained using electroproduction methods and neutrino scattering experiments [BEM02] respectively [4]. This results in a graph whose slope is much flatter than it should be. [Ale09] has the same problem with Fig. 2.4 showing the comparison between the physical and lattice dipole fits.

Before examining the possible reasons for this discrepancy, which we shall do so in later chapters, we look at another observable directly related to the form factor: the axial radius. In the next section we examine recent lattice results and see how they compare with experiment.

2.4 Axial Radius

While much effort has gone into finding the correct form of $G_A(Q^2)$ on the lattice, the axial radius $\langle r_A^2 \rangle$ has also been explored. The axial radius measures the spatial distribution of the axial current in the nucleon [You] and can be found relatively simply from the slope of the axial form factor at $Q^2 = 0$.[5] If we look at the expansion of the axial form factor,

$$G_A(Q^2) = g_A(1 - \frac{\langle r_A^2 \rangle}{6} Q^2) + \mathcal{O}(Q^4), \tag{2.41}$$

where $g_A = G_A(Q^2 = 0)$ is the axial charge, we see that the axial radius can be worked out from the formula,

$$\langle r_A^2 \rangle = -\frac{6}{G_A(0)} \frac{d}{dQ^2} G_A(Q^2) \Big|_{Q^2=0}, \tag{2.42}$$

and therefore that the radius is proportional to the slope of $G_A(Q^2)$. Given then that the form factors found on the lattice were all too flat we suspect that the $\langle r_A^2 \rangle$ values will be much smaller than the measured value. A look at Table 2.1 confirms these suspicions, for the experimental value of ≈ 0.44 fm^2 (using neutrino scattering techniques) is much larger than any of these values. A plot from [OY08] shows similar results,

Given the nature of the relationship between the axial form factor and the axial radius, if we could explain the discrepancy with the axial form factor, then it is most likely that we would have found an explanation for the

[4] This difference in experimental values is due to pion cloud effects[TW]. What the electroproduction methods actually measures is $\langle \tilde{r}_A^2 \rangle = \langle r_A^2 \rangle + \frac{3}{64 f_\pi} \left(1 - \frac{12}{\pi^2}\right)$.

[5] The radius can also be found from the electric dipole amplitude for $ep \to e'\pi^+ n$ in the limit that $m_\pi = 0$ [TW].

NOTE:
This table is included on page 17
of the print copy of the thesis held in
the University of Adelaide Library.

Table 2.1: Axial radius at different pion masses [B+10].

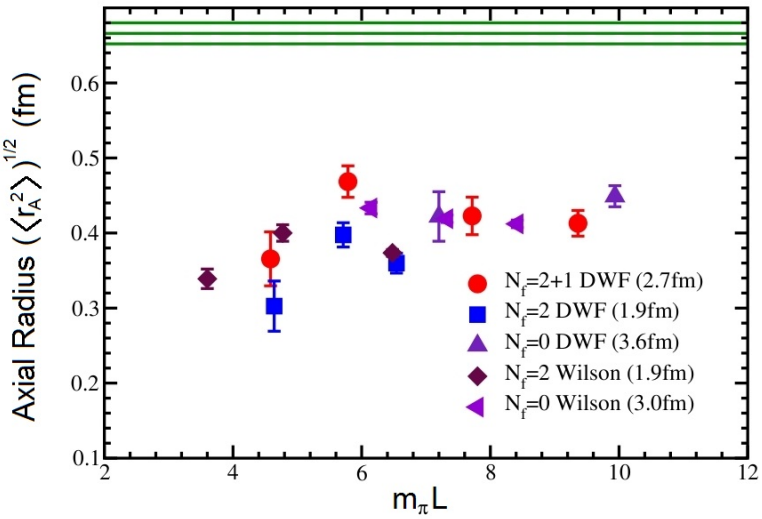

Figure 2.7: Axial radius for different values of $m_\pi L$ using domain wall fermions (DWF) and Wilson fermions. The solid lines show the experimental value [OY08].

problem with the axial radius as well. In the next few chapters this is what we seek to do.

* * *

Lattice results for the axial form factor consistently come up with values that are significantly different from experimental results. Due to the fact that larger lattice configurations are computational expensive much smaller ones have to be use. We suspect that the finite nature of the lattice is part of the reason behind this discrepancy.

In order to provide evidence for our suspicions we will look at a chiral model of the nucleon and examine the volume dependence of its axial form factor. Before we can proceed in this direction however, we must first provided some background on the chiral theory of QCD. As well as that we will discuss a number of other models in order to allow the reader to see where our choice sits in the scheme of things.

Chapter 3

Chiral Bag Models

In order to explain the discrepancy in the previous chapter we will be using an idealised model of the nucleon known as the "hedgehog". Without delving into the specifics of the solutions of this model (that is saved for the next chapter) we hope to provide a good understanding of the background ideas to the theory which governs this object.

No theory or model exists in a vacuum [DD] and so we will also discuss some other models which have gone before, and come after the hedgehog - providing the setting in which the hedgehog lies.

As chiral symmetry is such an important concept in this topic we will spend some time discussing the nature of this symmetry. We will also show its relation to the models being used and why it is necessary to include it.

Perhaps the best place to start is with chiral symmetry itself. Afterwards, as we start examining the models we can then include the model's relation to this symmetry much more smoothly.

3.1 Chiral symmetry

The Lagrangian density for QCD is,

$$\mathcal{L} = \bar{\psi}_q^i (i\gamma^\mu D_\mu^{ij} - \delta^{ij} m_q)\psi_q^j - \frac{1}{4} F_{\mu\nu}^a F^{a\,\mu\nu}\,, \tag{3.1}$$

where $F_{\mu\nu}$ is the non-abelian field tensor,

$$F_{\mu\nu}^a = \partial_\mu A_\nu^a - \partial_\nu A_\mu^a - g f_{abc} A_\mu^b A_\nu^c\,, \tag{3.2}$$

and D_μ^{ij} is the covariant derivative defined as,

$$D_\mu^{ij} = \delta^{ij}\partial_\mu + \frac{ig}{2}\lambda^{a\,ij} A_\mu^a\,. \tag{3.3}$$

The i, j indices label the three colours, q, the six quark flavours and a, the eight gluon fields. g is the strong coupling constant and f_{abc} the structure constants which come from the commutation relations between fields. The generators of the symmetry group are $\lambda^{a\,ij}$ and as usual we use the Einstein summation convention where like indices are summed over.

Under the following global *chiral* transformations,

$$\psi \;\rightarrow\; \psi - \frac{i}{2}\vec{\tau}\cdot\vec{\alpha}\,\gamma_5\,\psi\,; \tag{3.4}$$

$$\bar{\psi} \;\rightarrow\; \bar{\psi} - \frac{i}{2}\bar{\psi}\,\gamma_5\,\vec{\tau}\cdot\vec{\alpha}\,, \tag{3.5}$$

with ψ now a doublet including only the up and down quark flavours,

$$\psi = \begin{pmatrix} u \\ d \end{pmatrix}. \tag{3.6}$$

This Lagrangian remains invariant in the case where the quark masses are set to zero[1]. Substituting the transformed fields into Eq. (3.1),

$$\begin{aligned}
\mathcal{L} \;&\rightarrow\; \mathcal{L}' \\
&=\; (\bar{\psi} - \frac{i}{2}\bar{\psi}\,\gamma_5\,\vec{\tau}\cdot\vec{\alpha})^i_q\, i\gamma^\mu D^{ij}_\mu (\psi - \frac{i}{2}\vec{\tau}\cdot\vec{\alpha}\,\gamma_5\,\psi)^j_q - \frac{1}{4}F^a_{\mu\nu}F^{a\,\mu\nu} \\
&=\; \bar{\psi}^i_q\, i\gamma^\mu D^{ij}_\mu\,\psi^j_q - \frac{i^2}{2}(\bar{\psi}\,\gamma_5\,\vec{\tau}\cdot\vec{\alpha})^i_q\gamma^\mu D^{ij}_\mu\,\psi^j_q \\
&\qquad\qquad -\frac{i^2}{2}\bar{\psi}^i_q\,\gamma^\mu D^{ij}_\mu(\vec{\tau}\cdot\vec{\alpha}\,\gamma_5\,\psi)^j_q - \frac{1}{4}F^a_{\mu\nu}F^{a\,\mu\nu} + \mathcal{O}(\alpha^2) \\
&=\; \mathcal{L} + \frac{1}{2}\bar{\psi}^i_{q'}(\vec{\tau}\cdot\vec{\alpha})_{q'q}(\gamma_5\gamma^\mu + \gamma^\mu\gamma_5)D^{ij}_\mu\,\psi^j_q\,.
\end{aligned}$$

Then using the anticommutation relation,

$$\{\gamma_5, \gamma^\mu\} = 0\,, \tag{3.7}$$

we find that $\mathcal{L}' = \mathcal{L}$. This is known as chiral symmetry. Now the quark masses in the real world actually have finite masses and this means that the symmetry is broken. Nevertheless this is still a good approximation - accurate to within 7% [Pag75].

From Noether's theorem, we know that for every symmetry found in nature there is a conserved current associated with it. In this case our conserved currents are,

$$\vec{\mathrm{V}}^\mu = \bar{\psi}\gamma^\mu\vec{\tau}\psi\,; \tag{3.8}$$

$$\vec{\mathrm{A}}^\mu = \bar{\psi}\gamma^\mu\gamma_5\vec{\tau}\psi\,. \tag{3.9}$$

[1]Since the gluon fields, A^a_μ, live in colour space they are not affected by the transformation. For the same reason the covariant derivative also remains invariant.

These two currents are often combined in the form V ± A i.e. ,

$$\vec{\mathrm{L}}^{\mu} = \bar{\psi}\gamma^{\mu}(1-\gamma_5)\vec{\tau}\psi\,; \tag{3.10}$$

$$\vec{\mathrm{R}}^{\mu} = \bar{\psi}\gamma^{\mu}(1+\gamma_5)\vec{\tau}\psi\,, \tag{3.11}$$

where $\vec{L}^{\mu}$ and $\vec{R}^{\mu}$ are the left and right-handed quark currents respectively. QCD is then described as containing chiral $\mathrm{SU(2)_L \times SU(2)_R}$ symmetry. Another way to put it is to say that the left and right-handed particles do not mix [Tho84]. As the QCD Lagrangian is not exactly symmetric when masses are included the axial current is only *partially* conserved. This leads to the *partially conserved axial current* (PCAC) theorem.

PCAC

In Ref. [Col] Coleman explains that the "*PCAC is the statement that the matrix elements of* $\partial_\mu A^\mu$ *are ...* normally varying ". This means that these matrix elements are proportional to m_π^2 and so will go to zero in the limit $m_q \to 0$ [TW].

Looking at Eq. (2.32) again,

$$\langle\, \mathrm{B}\,|\vec{j}^{\mu 5}(q)|\,\mathrm{B}\,\rangle \;=\; \bar{u}\left[G_{\mathrm{A}}(q^2)\gamma^{\mu}\,\gamma^5 + \frac{i\sigma_{\mu\nu}q_\nu}{2m}\gamma^5 G_{\mathrm{T}}(q^2) + q^{\mu}\gamma^5 G_{\mathrm{P}}(q^2)\right]\vec{\tau}u\,, \tag{2.32}$$

if we contract both sides with q^μ and ignore quark masses for now we have

$$\begin{aligned} 0 &= \bar{u}\left[G_{\mathrm{A}}(q^2)\not{q}\,\gamma^5 + q^2\gamma^5 G_{\mathrm{P}}(q^2)\right]\vec{\tau}u \\ &= \bar{u}\left[G_{\mathrm{A}}(q^2)2m_N\,\gamma^5 + q^2\gamma^5 G_{\mathrm{P}}(q^2)\right]\vec{\tau}u \end{aligned} \tag{3.12}$$

and therefore[PS],

$$g_A = \lim_{q^2\to 0}\frac{q^2}{2m_N}G_{\mathrm{P}}(q^2)\,. \tag{3.13}$$

This equation would cause problems if it were not for the pole $G_{\mathrm{P}}(q^2)$ - illustrated in Fig. 3.1. By including the pole we end up with the *Goldberger-Treimann relation*:

$$g_A = \frac{f_\pi}{m_N}g_{\pi NN}. \tag{3.14}$$

So the PCAC leads necessarily to the production of a pion. Let us now turn to another issue involving chiral symmetry.

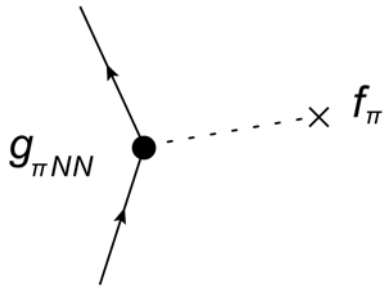

Figure 3.1: Pion pole contribution to the pseudoscalar form factor [TW].

* * *

As we showed above, the axial current is conserved when the quarks are massless. This means that the axial charge commutes with the Hamiltonian,

$$[\mathrm{Q}_A, \mathrm{H}] = 0. \tag{3.15}$$

From this it follows that if an eigenstate of H with positive parity exists, then there must also exist a corresponding state of negative parity with the same mass [Tho84, You04] i.e. if,

$$\mathrm{H}|N^+\rangle = m|N^+\rangle. \tag{3.16}$$

then with,

$$|N^-\rangle = \mathrm{Q}_A|N^+\rangle \tag{3.17}$$

we end up with,

$$\begin{aligned} \mathrm{H}|N^-\rangle &= \mathrm{HQ}_A|N^+\rangle \\ &= \mathrm{Q}_A\mathrm{H}|N^+\rangle \\ &= \mathrm{Q}_A m|N^+\rangle \\ &= m|N^-\rangle\,. \end{aligned} \tag{3.18}$$

The nucleon is an eigenstate of H with positive parity, however no such particle of $m \approx 940$ MeV exists with negative parity. The closest that exist are the N(1535) and $\Delta(1620)$ and these are over 600 MeV heavier [You04]. Clearly this must be resolved before we can accept seriously the assumption that chiral symmetry is reliable.

The solution is provided by Goldstone, who, in the theorem named after him, showed that when a symmetry is broken a particle of zero spin and zero mass must be produced [Gol61]. These particles are known as Goldstone bosons. In the case of negative parity states then, what we have is a

mixture of the nucleon and the Goldstone bosons [Tho84, You04]. For QCD the pions are considered to be the approximation of these Goldstone particles - approximate because they actually have a small mass.

* * *

In summary, the agreement between the theory and experiment provides evidence that chiral symmetry is a good symmetry of QCD [Pag75]. We showed how for massless quarks the QCD Lagrangian is invariant. We also looked at how the conservation of axial current was preserved by inclusion of a Goldstone boson which in the case of QCD is the pion.

As a result of these factors, when people began to construct a model of the nucleon, one of the important features they tried to include was chiral symmetry. In the next few sections we will examine what these models were and how they incorporated (or failed to incorporate) chiral symmetry.

3.2 MIT Bag Model

By the time of the construction of the MIT bag model, confinement and asymptotic freedom had become fundamental tenants of QCD. Quarks were known to behave freely in the high energy state while at low energies the increase in the strong coupling constant, α_s, prevented them from being seen individually.

It was the desire to incorporate these features of QCD in a covariant manner that produced the MIT bag model [CJJT74, DJJK75]. The MIT bag model successfully predicted the value of the axial coupling constant as well as providing reasonably good results for the baryon masses. These are shown in Fig. 3.2.

However, there were some problems with it too. The model failed to produce the right values for the charge radius and magnetic moments [Tho84]. It also suffered from the fact that chiral symmetry was *explicitly* broken.

The Lagrangian of the MIT bag model is,

$$\mathcal{L}_{\rm MIT} = (i\bar{\psi}\gamma^\mu\partial_\mu\psi - B)\theta_{\rm V} - \frac{1}{2}\bar{\psi}\psi\delta_{\rm S}\,, \tag{3.19}$$

where,

$$\theta_{\rm V} = \begin{cases} 1 & \text{inside the bag} \\ 0 & \text{outside} \end{cases} \tag{3.20}$$

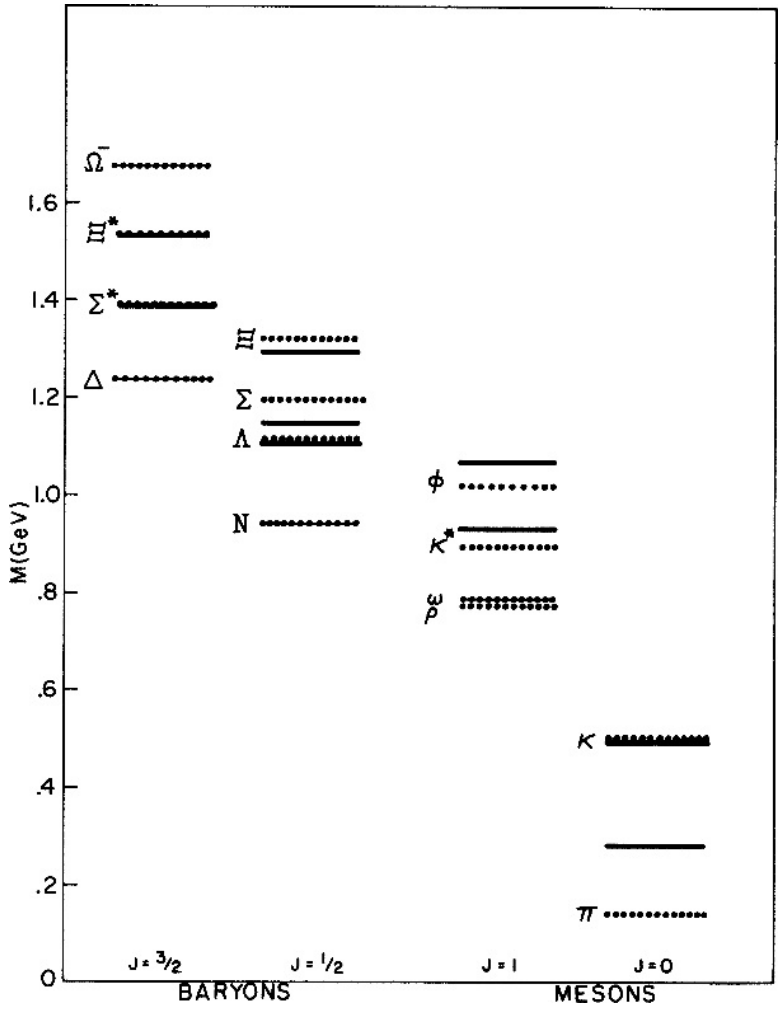

Figure 3.2: MIT bag model baryon mass spectrum [DJJK75]. The dotted lines are the experimental values, the thick lines the bag model predictions, and the thin lines were the masses used to set model parameter.

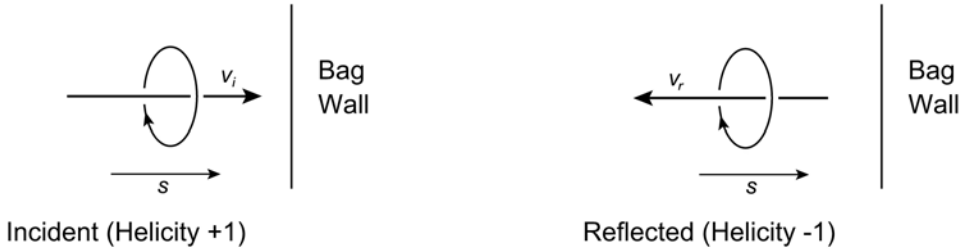

Figure 3.3: Chiral symmetry breaking at the surface of the bag [Tho84, Gri].

and $\delta_{\rm S}$ is a surface delta function. By applying the same transformations (Eqs. (3.4) and (3.5)) used on the QCD Lagrangian, we see that there is an extra term which breaks the invariance of $\mathcal{L}_{\rm MIT}$.

$$\begin{aligned}
\mathcal{L}_{\rm MIT} \rightarrow \mathcal{L}'_{\rm MIT} &= [i(\bar{\psi} - \frac{i}{2}\bar{\psi}\,\gamma_5\,\vec{\tau}\cdot\vec{\alpha})\gamma^\mu\partial_\mu(\psi - \frac{i}{2}\vec{\tau}\cdot\vec{\alpha}\,\gamma_5\,\psi) - B]\theta_{\rm V} \\
&\quad -\frac{1}{2}(\bar{\psi} - \frac{i}{2}\bar{\psi}\,\gamma_5\,\vec{\tau}\cdot\vec{\alpha})(\psi - \frac{i}{2}\vec{\tau}\cdot\vec{\alpha}\,\gamma_5\,\psi)\delta_{\rm S} \\
&= \mathcal{L}'_{\rm MIT} + \frac{1}{2}\bar{\psi}(\gamma_5\gamma^\mu + \gamma^\mu\gamma_5)\vec{\tau}\cdot\vec{\alpha}\partial_\mu\psi + \frac{i}{2}\bar{\psi}\gamma_5\vec{\tau}\cdot\vec{\alpha}\psi\delta_{\rm S} \\
&= \mathcal{L}'_{\rm MIT} + \frac{i}{2}\bar{\psi}\gamma_5\vec{\tau}\cdot\vec{\alpha}\psi\delta_{\rm S}\,, \qquad (3.21)
\end{aligned}$$

Thomas in Ref.[Tho84] puts it this way:

Confinement implies that any quark impinging on the bag surface must be reflected. However, there is no spin-flip associated with the reflection, and hence the chirality, or handedness of the quarks is changed.

Fig. 3.3 shows this explicitly. As a result of all these problems, the physicists working on the model quickly began to look for ways to solve this problem. In the next section we look at one of these attempts: the σ-model.

3.3 The σ-model

Another representation of the nucleon, slightly different from the bag models of the nucleon is the σ-model. Invented by Gell-Mann and Levy in the 1960s the σ-model was used to reconcile the heavy mass of the nucleon with the fact that the axial current is partially conserved [Tho84].

The essential features of this model are the extra $\vec{\pi}$ and σ fields. By defining these fields to transform as,

$$\sigma \rightarrow \sigma - \vec{\alpha}\cdot\vec{\pi}\,; \tag{3.22}$$
$$\vec{\pi} \rightarrow \vec{\pi} + \sigma\vec{\alpha}\,, \tag{3.23}$$

and replacing the mass term with $g\bar{\psi}(\sigma + i\vec{\tau}\cdot\vec{\pi}\gamma_5)\psi$ chiral symmetry is restored.

The Lagrangian for this model is thus [Tho84],

$$\begin{aligned}\mathcal{L}_\sigma &= i\bar{\psi}\gamma^\mu\partial_\mu\psi + g\bar{\psi}(\sigma + i\vec{\tau}\cdot\vec{\pi}\gamma_5)\psi + \frac{1}{2}(\partial_\mu\sigma)^2 + \frac{1}{2}(\partial_\mu\vec{\pi})^2 \\ &- \frac{\lambda^2}{4}\left((\sigma^2+\vec{\pi}^2) - \nu^2\right)\,. \end{aligned}\tag{3.24}$$

Spontaneous symmetry breaking then produces the required mass term for the nucleon.

Unfortunately the σ-model cannot be taken as a serious representation of QCD. Instead of treating the nucleon as a complex combination of quarks and gluons, the sigma model makes out the nucleon to be a point particle. On top of the that, the axial charge g_A is assumed to be equal to 1, when experimentally it has been found to be 1.27.

Having now seen the σ-model and explained some of its characteristics, we turn our attention to another model - the hedgehog.

3.4 Hedgehog Model

Soon after the MIT bag model was produced, Chodos and Thorn [CT75] (and also Inoue and Maskawa [IM75]) created a model which incorporated chiral symmetry. Like the sigma model, new fields σ and $\vec{\pi}$ are introduced although in this case they included in the MIT surface term. This can be seen explicitly in [CT75],

$$\mathcal{L}_{\rm CT} = (i\bar{\psi}\gamma^\mu\partial_\mu\psi - B)\theta_{\rm V} - \lambda\bar{\psi}(\sigma + i\vec{\tau}\cdot\vec{\pi}\gamma_5)\psi\delta_{\rm S} + \frac{1}{2}(\partial_\mu\sigma)^2 + \frac{1}{2}(\partial_\mu\pi)^2\,, \tag{3.25}$$

where $\lambda = \frac{1}{2}(\sigma^2+\vec{\pi}^2)^{-\frac{1}{2}}$ is a Lagrangian multiplier. We leave this as an exercise to show that this expression is invariant under chiral transformations.

One of the important things to note from the Lagrangian is the fact that both the σ and $\vec{\pi}$ fields couple only to the surface of the bag. This

means that except for when they interact with the bag's surface they behave as free fields.

The beauty of this Lagrangian is that its equations of motion can be solved exactly. However, this is somewhat tempered by the fact that the physical nature of the solution is questionable. When Chodos and Thorn solved these equations, what they found was a rather idealistic baryon - one which was neither an eigenstate of spin or isospin. The wave function of this baryon is proportional to [CT75],

$$|h\rangle = |\chi_h\rangle_1 |\chi_h\rangle_2 |\chi_h\rangle_3 \tag{3.26}$$

where,

$$|\chi_h\rangle = \frac{1}{\sqrt{2}}(|u\downarrow\rangle - |d\uparrow\rangle)\,. \tag{3.27}$$

Obviously no such state has ever been observed in experiments. Despite this, the hedgehog has been used to study the features of the nucleon. This is mainly due to the fact that it is possible to extract exact solutions [CT75].

For the massless case, the solutions Chodos and Thorn found were,

$$q(\vec{r}) = \begin{pmatrix} j_0\left(\frac{\Omega r}{R}\right) \\ i\vec{\sigma}\cdot\hat{r}j_1\left(\frac{\Omega r}{R}\right) \end{pmatrix} \chi_h e^{-i(\Omega/R)t} \tag{3.28}$$

$$\sigma(\vec{r}) = f(r) \tag{3.29}$$

$$\vec{\pi}(\vec{r}) = g(r)\hat{r}, \tag{3.30}$$

where j_0 and j_1 are spherical Bessel functions, Ω is the bag frequency, and R is the radius of the bag. This radial dependence we see in the solutions is the origin of the name - if we were to draw a diagram of the spin (or isospin) fields then they would look rather like a pin-cushion or a "real-life" hedgehog.

Thomas *et al.* used the hedgehog in [TALY05] to study the finite volume properties of the axial charge g_A. We will follow their use of the hedgehog in order to extend it to the study the axial form factor. As opposed to Chodos and Thorn who solved for the massless case, Thomas *et al.* found solutions for massive quarks and pions which we also use. Before we do that though, there is one more model that we need to describe. This model also respects chiral symmetry and does not suffer from the problem of the hedgehog which produces a rather abstract view of the nucleon. This last model is the cloudy bag model.

3.5 The Cloudy Bag Model

The cloudy bag model (CBM) [TTM80, TTM81, MTT81] grew up out of the attempt to solve the problems of a non-linear version of the MIT bag model[2]. Like the MIT (and hedgehog) model, the quarks are confined to a "bag" of specified radius denoted here as R. As in the case of the hedgehog a new field, designated $\vec{\phi}$, is introduced to preserve chiral symmetry. This pion field is allowed to move both inside and outside the bag.

The Lagrangian density for the CBM is given as [TTM80, DeT81],

$$\begin{aligned}\mathcal{L}_{\rm CBM} &= (i\bar{\psi}\gamma^\mu\partial_\mu\psi - B)\theta_{\rm V} - \frac{1}{2}\bar{\psi}\psi\delta_{\rm S} + \frac{1}{2}(\partial_\mu\vec{\phi})^2 \\ &\quad -\frac{1}{2}m_\pi^2(\vec{\phi})^2 - \frac{i}{2f_\pi}\bar{\psi}\gamma_5\vec{\tau}\cdot\vec{\phi}\,\psi\,\delta_{\rm S}\,, \end{aligned} \tag{3.31}$$

where f_π is the pion decay constant and the extra mass term $\frac{1}{2}m_\pi^2(\vec{\phi})^2$ breaks the exact chiral symmetry and leaves the axial current partially conserved - as is the case in the real world.

The pions themselves are assumed to have a large Compton wavelength and this means that perturbation theory can be used [Tho84]. This is true as long as the pion "cloud" around the nucleon contains only a small number of particles and the bag radius is large (≥ 0.7 fm) [TW].

The CBM has produced impressive results. The root-mean-square radius, magnetic moment of the nucleon, and g_A are all in good agreement with experiment [TTM81]. In fact the calculated magnetic moments of all the baryon octets agree well with measured values which we can see in Fig. 3.4.

An extra transformation on the $\mathcal{L}_{\rm CBM}$

$$\psi \rightarrow \psi_w = S\psi \tag{3.32}$$

$$\bar{\psi} \rightarrow \bar{\psi}_w = \bar{\psi}S \tag{3.33}$$

where

$$S = \exp(\frac{i\vec{\tau}\cdot\vec{\phi}\gamma_5}{2f_\pi}), \tag{3.34}$$

gives a new form of the Lagrangian [Tho84]:

$$\begin{aligned}\mathcal{L}'_{\rm CBM} &= (i\bar{\psi}_w\partial\!\!\!/\psi_w - B)\theta_{\rm V} - \frac{1}{2}\bar{\psi}_w\psi_w\delta_{\rm S} - \frac{\theta_{\rm V}}{4f_\pi^2}\bar{\psi}_w\gamma^\mu\vec{\tau}\cdot(\vec{\phi}\times\partial_\mu\vec{\phi})\phi_w \\ &\quad +\frac{\theta_{\rm V}}{2f_\pi}\bar{\psi}_w\gamma^\mu\gamma_5\vec{\tau}\cdot\partial_\mu\vec{\phi}\psi_w + \frac{1}{2}(\partial_\mu\vec{\phi})^2 - \frac{1}{2}m_\pi^2(\vec{\phi})^2\,. \end{aligned} \tag{3.35}$$

[2]See the lectures by Jaffe in Ref. [Jaf].

	CBM	Experiment
p	2.60[a]	2.793
n	−2.01[a]	−1.913
Λ	−0.58	−0.614 ± 0.005
Σ^-	−1.08	−1.41 ± 0.27
Σ^+	2.34	2.33 ± 0.13
Ξ^-	−0.51	−0.75 ± 0.07[b]
Ξ^0	−1.27	−1.25 ± 0.014

Figure 3.4: CBM model baryon magnetic moments [TT83]. For a) $R = 0.82$ was used from [TTM81]. b) A preliminary result at the time [TT83] was published.

* * *

In this chapter we have described a number of different models used to represent the nucleon. We looked at the MIT bag model and how its failure to include chiral symmetry meant it was not a viable option. We looked at the σ-model and saw how it treated the nucleon only as a point particle thus loosing the complexity of QCD. Finally we reviewed the cloudy bag model. Ideally we would use the CBM to study the nucleon's axial form factor rather than the hedgehog. However, as mentioned before, the hedgehog has an exact solution making it more fitting for use in this thesis.

Chapter 4

Hedgehog Calculations

We are now close to the point where we calculate the axial form factor of the hedgehog. From Eqs. (3.28), (3.29) and (3.30) we know the general form of the field solutions; substituting these into the matrix element involving the axial current, Eq. (2.32), would then give the axial form factor. However, Refs. [CT75] and [TALY05] have shown it is possible to find exact, analytic solutions and it is beneficial to look at these background calculations first. Once we have understood these we can move on to the challenge of finding the form factor; this occurs in the second section.

The axial radius is another important observable to be discussed. In the final section we examine its relationship to the form factor - looking at both dipole and gradient methods for extracting a value from the lattice data. It is important to note that for both the axial form factor and the axial radius, calculations were made for several different configurations of pion mass and lattice volume.

Finally, we must make mention of the special use of the lattice side-length L. Conventionally the lattice is a four dimensional "box" or hypercube with side length L. In our case we make use of the fact that we are dealing with radially symmetric solutions and instead use a 4-D "sphere". L then becomes the radius of this sphere. We will often use the diameter, $d = 2L$, as a measure as well. Although this complicates how we understand the boundary conditions, it allows us to introduce volume dependence much more simply.

4.1 Background

Most of the initial work in this section has already been done in Refs. [CT75] and [TALY05]. Chodos and Thorn solved the equations of motion for the

massless case, while Thomas *et al.* did the same with quark and pion masses included. This section provides an overview of their work.

We start with [TALY05],

$$\begin{aligned}\mathcal{L} &= [\bar{\psi}(i\partial\!\!\!/ - m_q)\psi - B]\theta_V - \lambda\bar{\psi}\left(\sigma + i\vec{\tau}\cdot\vec{\pi}\gamma_5\right)\psi\delta_S \\ &\quad + \frac{1}{2}\left(\partial_\mu\sigma\right)\left(\partial^\mu\sigma\right) + \frac{1}{2}\left(\partial_\mu\vec{\pi}\right)\cdot\left(\partial^\mu\vec{\pi}\right) - \frac{1}{2}m_\pi^2\vec{\pi}\cdot\vec{\pi}\,. \qquad (4.1)\end{aligned}$$

where we have included the mass terms in the Lagrangian. As is the case in all our models, the quarks have been confined to the inside of a spherical bag of radius R; this is enforced by θ_V. The δ_S is a surface delta function which guarantees that the σ and $\vec{\pi}$ fields couple to the quark fields only at the surface. Energy-momentum conservation through the surface of the bag is ensured with B - an energy density term which we will put in explicitly. Finally, λ is a Lagrange multiplier equal to $\frac{1}{2}(\sigma^2 + \vec{\pi}^2)^{-\frac{1}{2}}$.

Using Hamilton's principle of least action, i.e. requiring that:

$$\delta S = 0 \qquad (4.2)$$

we obtain the following Euler-Lagrange equations [TALY05]

$$\begin{aligned}\left(i\partial\!\!\!/ - m_q\right)\psi &= 0, \qquad r < R; & (4.3)\\ \nabla^2\sigma &= \frac{1}{2}\xi\bar{\psi}\psi\delta(r-R); & (4.4)\\ \nabla^2\vec{\pi} - m_\pi^2\vec{\pi} &= \frac{1}{2}\xi\bar{\psi}i\vec{\tau}\gamma_5\psi\delta(r-R); & (4.5)\\ i\hat{r}\cdot\vec{\gamma}\psi &= -\xi\left(\sigma + i\vec{\tau}\cdot\vec{\pi}\gamma_5\right)\psi, \qquad r = R; & (4.6)\\ B &= -\frac{1}{2}\xi\frac{\partial}{\partial r}\left[\bar{\psi}\left(\sigma + i\vec{\tau}\cdot\vec{\pi}\gamma_5\right)\psi\right]_{r=R}\,, & (4.7)\end{aligned}$$

where $\xi = [(\sigma^2(R) + \vec{\pi}^2(R)]^{-\frac{1}{2}}$; and we are now considering a *static* spherical bag. The first three are the equations of motion of the q, σ and $\vec{\pi}$ fields, while the last two are boundary conditions.

Returning to all four dimensions for a moment, we see that Eq. (4.6), along with our original Lagrangian, implies quark confinement. Starting with,

$$in\cdot\vec{\gamma}\psi = -\xi\left(\sigma + i\vec{\tau}\cdot\vec{\pi}\gamma_5\right)\psi, \qquad r = R\,, \qquad (4.6)$$

with n_μ the normal vector and taking the Hermitian conjugate we have,

$$\begin{aligned}\left(in\cdot\vec{\gamma}\psi\right)^\dagger &= -\left[\xi\left(\sigma + i\vec{\tau}\cdot\vec{\pi}\gamma_5\right)\psi\right]^\dagger\,, \\ -i\psi^\dagger n\cdot\gamma^\dagger &= -\psi^\dagger(-i\gamma_5^\dagger\vec{\tau}\cdot\vec{\pi} + \sigma)\xi\,.\end{aligned}$$

If we now multiply both sides on the right by γ^0 the above equation becomes,

$$\begin{aligned} -i\psi^\dagger n\cdot\gamma^\dagger\gamma^0 &= -\psi^\dagger(-i\gamma_5^\dagger\vec{\tau}\cdot\vec{\pi}+\sigma)\xi\gamma^0 \\ i\bar{\psi}\gamma\cdot n &= \bar{\psi}(i\gamma_5\vec{\tau}\cdot\vec{\pi}+\sigma)\xi\,. \end{aligned} \tag{4.8}$$

Then taking the product of the quark current $j^\mu=\bar{\psi}\gamma^\mu\psi$ with n_μ we have [Tho84],

$$\begin{aligned} in_\mu j^\mu &= \bar{\psi}i\gamma\cdot n\psi \\ &= (\bar{\psi}i\gamma\cdot n)\psi = [\bar{\psi}(\gamma_5\vec{\tau}\cdot\vec{\pi}+\sigma)\xi]\psi \\ &= \bar{\psi}(i\gamma\cdot n\psi) = -\bar{\psi}[\xi(\sigma+i\vec{\tau}\cdot\vec{\pi}\gamma_5)\psi] \\ &= 0\,. \end{aligned}$$

This means that there is no quark current coming out of the bag and thus the quarks must be confined. The last equation, Eq. (4.7), is the non-linear boundary condition which ensures that the pressure created by the free quarks inside the bag is matched by the outside pressure [TW].

The solutions to these equations are similar to the ones we showed before, however, there are now a few extra terms stemming from the fact that quark and pion masses are now present. The new solutions are [TALY05],

$$\psi(\vec{r}) = \begin{pmatrix} \alpha_+ j_0\left(\frac{\Omega r}{R}\right) \\ i\alpha_-\vec{\sigma}\cdot\hat{r}\,j_1\left(\frac{\Omega r}{R}\right) \end{pmatrix}\chi_h\theta(R-r)e^{-i\alpha t/R} \tag{4.9}$$

$$\sigma(\vec{r}) = f(r) \tag{4.10}$$

$$\vec{\pi}(\vec{r}) = g(r)\hat{r}, \tag{4.11}$$

with

$$\alpha = ER = \sqrt{\Omega^2+(m_qR)^2} \tag{4.12}$$

and

$$\alpha_\pm = \sqrt{\frac{\alpha\pm m_qR}{\alpha}}\,. \tag{4.13}$$

Substituting these solutions into the equations of motion, beginning with the sigma field equation,

$$\nabla^2\sigma = \frac{1}{2}\xi\bar{\psi}\psi\delta(r-R); \tag{4.4}$$

the left-hand side becomes,

$$\begin{aligned} L.H.S. &= \frac{1}{2}\xi\bar{\psi}\psi\delta(r-R) \\ &= \frac{1}{2}\xi e^{-i\alpha t/R}\chi_h^\dagger(\alpha_+ j_0(\Omega), -i\alpha_- j_1(\Omega)\vec{\sigma}\cdot\hat{r}) \begin{pmatrix} 1 & 0 \\ 0 & -1 \end{pmatrix} \begin{pmatrix} \alpha_+ j_0(\Omega) \\ i\alpha_-\vec{\sigma}\cdot\hat{r}j_1(\Omega) \end{pmatrix} \\ &\quad .\chi_h\theta(R-r)e^{-i\alpha t/R}\delta(r-R) \\ &= \chi_h^\dagger[\alpha_+^2 j_0^2(\Omega) - \alpha_-^2 j_1^2(\Omega)(\vec{\sigma}\cdot\hat{r})^2]\chi_h\theta(R-r)\delta(r-R) \\ &= \frac{1}{2}\xi(\alpha_+^2 j_0^2(\Omega) - \alpha_-^2 j_1^2(\Omega))\chi_h^\dagger\chi_h\delta(R-r), \end{aligned} \tag{4.14}$$

while the right-hand side,

$$\begin{aligned} R.H.S. &= \nabla^2\sigma \\ &= \nabla^2 f(r) \\ &= \frac{1}{r^2}\frac{\partial}{\partial r}r^2\frac{\partial}{\partial r}f + 0 + 0 \\ &= \frac{2}{r}f' + f''. \end{aligned} \tag{4.15}$$

Combining the two we end up with [TALY05],

$$\begin{aligned} f''(r) + \frac{2}{r}f'(r) &= \frac{1}{2}\xi(\alpha_+^2 j_0^2(\Omega) - \alpha_-^2 j_1^2(\Omega))\chi_h^\dagger\chi_h\delta(R-r) \\ &\equiv a\delta(R-r). \end{aligned} \tag{4.16}$$

Similarly, if we look at the pion field equation:

$$\nabla^2\vec{\pi} - m_\pi^2\vec{\pi} = \frac{1}{2}\xi\bar{\psi}i\vec{\pi}\gamma_5\psi\delta(r-R), \tag{4.5}$$

then the left-hand side under substitution becomes,

$$\begin{aligned} L.H.S. &= \frac{1}{2}\xi i e^{-i\alpha t/R}\chi_h^\dagger(\alpha_+ j_0(\Omega), -i\alpha_- j_1(\Omega)\vec{\sigma}\cdot\hat{r}) \begin{pmatrix} 1 & 0 \\ 0 & -1 \end{pmatrix} \\ &\quad \cdot \begin{pmatrix} \vec{\tau} & 0 \\ 0 & \vec{\tau} \end{pmatrix} \begin{pmatrix} 0 & 1 \\ 1 & 0 \end{pmatrix} \begin{pmatrix} \alpha_+ j_0(\Omega) \\ i\alpha_-\vec{\sigma}\cdot\hat{r}j_1(\Omega) \end{pmatrix} \chi_h\theta(R-r)e^{-i\alpha t/R}\delta(r-R) \\ &= i\chi_h^\dagger(\alpha_+ j_0(\Omega), -i\alpha_- j_1(\Omega)\vec{\sigma}\cdot\hat{r}) \begin{pmatrix} \vec{\tau}i\alpha_-\vec{\sigma}\cdot\hat{r}j_1(\Omega) \\ -\vec{\tau}\alpha_+ j_0(\Omega) \end{pmatrix} \chi_h\delta(r-R) \\ &= i\chi_h^\dagger\left[i\alpha_+ j_0(\Omega)\vec{\tau}\alpha_-\vec{\sigma}\cdot\hat{r}j_1(\Omega) + i\alpha_- j_1(\Omega)\vec{\sigma}\cdot\hat{r}\vec{\tau}\alpha_+ j_0(\Omega)\right]\chi_h\delta(r-R) \end{aligned} \tag{4.17}$$

Using $\chi_h^\dagger \tau_i \sigma_j \chi_h = -\delta_{ij}\chi_h^\dagger \chi_h$ this ends up as,

$$L.H.S. = \xi\alpha_+\alpha_- j_0(\Omega) j_1(\Omega)\chi_h^\dagger\chi_h \hat{r}\delta(r-R)\,. \tag{4.18}$$

With the right-hand side,

$$\begin{aligned} R.H.S. &= \nabla^2\vec{\pi} - m_\pi^2\vec{\pi} \\ &= \nabla^2(g(r)\hat{r}) - m_\pi^2 g(r)\hat{r} \\ &= g''(r)\hat{r} + \frac{2}{r}g'(r)\hat{r} - \frac{2}{r^2}g(r)\hat{r} - m_\pi^2 g(r)\hat{r} \end{aligned} \tag{4.19}$$

putting the two together the pion field equation becomes [TALY05],

$$\begin{aligned} g''(r) + \frac{2}{r}g'(r) - (\frac{2}{r^2} + m_\pi^2)g(r) &= \xi\alpha_+\alpha_- j_0(\Omega) j_1(\Omega)\chi_h^\dagger\chi_h\delta(R-r) \\ &\equiv b\delta(R-r). \end{aligned} \tag{4.20}$$

Two more conditions then help us to specify the solutions to these equations: regularity and periodicity. The lattice approximates the continuum by requiring that the hypercube should have periodic boundary conditions, this means that the value for the fields at L are equal to those at zero - remembering that L is the side-length. In essence what happens is that the hypercubes are stacked up together, each with a nucleon inside it. In our special case we implement it by demanding that the gradient of the pion be zero at the edge of the boundary, i.e.

$$\left.\frac{\partial\pi}{\partial r}\right|_{r=L} = 0\,. \tag{4.21}$$

Applying these two conditions gives the solutions [TALY05]

$$f(r) = f_0 + aR^2(\frac{1}{R} - \frac{1}{r})\theta(r-R) \tag{4.22}$$

$$\begin{aligned} g(r) &= b(R\cosh Rm_\pi - \frac{\sinh Rm_\pi}{m_\pi})(-\frac{\cosh rm_\pi}{rm_\pi} + \frac{\sinh rm_\pi}{r^2m_\pi^2})\Gamma(Lm_\pi) \\ &+ b(R\sinh Rm_\pi - \frac{\cosh Rm_\pi}{m_\pi})(\frac{\cosh rm_\pi}{rm_\pi} - \frac{\sinh rm_\pi}{r^2m_\pi^2})\theta(R-r) \\ &+ b(R\cosh Rm_\pi - \frac{\sinh Rm_\pi}{m_\pi})(\frac{\sinh rm_\pi}{rm_\pi} - \frac{\cosh rm_\pi}{r^2m_\pi^2})\theta(r-R)\,, \end{aligned} \tag{4.23}$$

with the volume dependence of the pion field being given by,

$$\Gamma(Lm_\pi) = \left(\frac{\frac{\cosh Lm_\pi}{Lm_\pi} - 2\frac{\sinh Lm_\pi}{L^2m_\pi^2} + 2\frac{\cosh Lm_\pi}{L^3m_\pi^3}}{\frac{\sinh Lm_\pi}{Lm_\pi} - 2\frac{\cosh Lm_\pi}{L^2m_\pi^2} + 2\frac{\sinh Lm_\pi}{L^3m_\pi^3}}\right)\,. \tag{4.24}$$

Note that it is the periodic b.c. which brings the volume dependence into $g(r)$.

It is also interesting to look at the case where instead of the gradient being zero, the pion field itself is set to zero. Beginning with the general solution of the pion field [TALY05],

$$\begin{aligned} g(r) &= b(R\sinh Rm_\pi - \frac{\cosh Rm_\pi}{m_\pi})(\frac{\cosh rm_\pi}{rm_\pi} - \frac{\sinh rm_\pi}{r^2m_\pi^2})\theta(R-r) \\ &+ b(R\cosh Rm_\pi - \frac{\sinh Rm_\pi}{m_\pi})(\frac{\sinh rm_\pi}{rm_\pi} - \frac{\cosh rm_\pi}{r^2m_\pi^2})\theta(r-R) \\ &+ (-\frac{\cosh rm_\pi}{rm_\pi} + \frac{\sinh rm_\pi}{r^2m_\pi^2})C\,, \end{aligned} \tag{4.25}$$

and applying the new b.c. $\vec{\pi} = 0$ at $r = L$ we have,

$$\begin{aligned} 0 &= b(R\cosh Rm_\pi - \frac{\sinh Rm_\pi}{m_\pi})(\frac{\sinh Lm_\pi}{Lm_\pi} - \frac{\cosh Lm_\pi}{L^2m_\pi^2}) \\ &+ (-\frac{\cosh Lm_\pi}{Lm_\pi} + \frac{\sinh Lm_\pi}{L^2m_\pi^2})C\,, \end{aligned} \tag{4.26}$$

where C is a constant. Rearranging this equation to get C,

$$C = \frac{b(R\cosh Rm_\pi - \frac{\sinh Rm_\pi}{m_\pi})(\frac{\sinh Lm_\pi}{Lm_\pi} - \frac{\cosh Lm_\pi}{L^2m_\pi^2})}{(-\frac{\cosh Lm_\pi}{Lm_\pi} + \frac{\sinh Lm_\pi}{L^2m_\pi^2})}\,, \tag{4.27}$$

substituting this expression for C back into Eq. (4.25) the result for the pion field is,

$$\begin{aligned} g(r) &= b(R\cosh Rm_\pi - \frac{\sinh Rm_\pi}{m_\pi})(-\frac{\cosh rm_\pi}{rm_\pi} + \frac{\sinh rm_\pi}{r^2m_\pi^2})\Gamma'(Lm_\pi) \\ &+ b(R\sinh Rm_\pi - \frac{\cosh Rm_\pi}{m_\pi})(\frac{\cosh rm_\pi}{rm_\pi} - \frac{\sinh rm_\pi}{r^2m_\pi^2})\theta(R-r) \\ &+ b(R\cosh Rm_\pi - \frac{\sinh Rm_\pi}{m_\pi})(\frac{\sinh rm_\pi}{rm_\pi} - \frac{\cosh rm_\pi}{r^2m_\pi^2})\theta(r-R)\,, \end{aligned} \tag{4.28}$$

where,

$$\Gamma'(Lm_\pi) = \left(\frac{\frac{\sinh Lm_\pi}{Lm_\pi} - \frac{\cosh Lm_\pi}{L^2m_\pi^2}}{\frac{\cosh Lm_\pi}{Lm_\pi} - \frac{\sinh Lm_\pi}{L^2m_\pi^2}}\right)\,. \tag{4.29}$$

We will see in the next chapter what effects these different boundary conditions have on the axial form factor.

The boundary condition for the sigma field is found using the PCAC relation:

$$\langle 0|\partial_\mu A_a^\mu(x)|\pi_b(q)\rangle = f_\pi m_\pi^2 \delta_{ab} e^{-iq\cdot x} \tag{4.30}$$

comparing this with the infinite volume case,

$$\langle 0|\partial_\mu A_a^\mu(x)|\pi_b(q)\rangle = \langle\sigma\rangle\, m_\pi^2 \delta_{ab} e^{-iq\cdot x}\,, \tag{4.31}$$

we see that $\langle\sigma\rangle = f_\pi$ as r goes to infinity. In order to set a boundary condition that approximates the lattice, we take the value of the sigma field at $r = L$ i.e. $\sigma(r = L)$ in the infinite volume solution and set this to be the value at the edge of the lattice [TALY05].

Once the field solutions have been placed in Eq. (4.7) and the derivatives on the right-hand side performed[1], the equation becomes,

$$4\pi R^4 B = \tau(\Omega, m_q, m_\pi, R, L)\,, \tag{4.32}$$

where τ is a rather complicated function not shown. Combining this with the solution for $f(r)$ at infinity:

$$\lim_{r\to\infty} f(r) = f_\pi = f_0(R,\Omega) + a(R,\Omega)R\,, \tag{4.33}$$

produces two eigenvalue equations, Eqs. (4.32) and (4.33) involving a number of parameters, m_q, m_π, B etc. To solve these two equations for R and Ω we substitute the values for the parameters. In our case we used a number of different values of m_π and then applied the Gell-Mann-Oakes-Renner relation $m_\pi^2 \propto m_q$ to work out the quark mass. B, the energy density is set to 13.97 MeV/fm^3

The solutions for the cases $L = 100$ fm and $L = 3$ fm are shown below[2]. Both the quark and the sigma fields show little variation. The pion field however, is much larger for the finite volume. This is because it has not had time to die off before it reaches the boundary of the lattice. As we shall see, this behaviour will become significant in our study of the axial form factor.

* * *

Although this section has been essential to our understanding of the hedgehog model, it is all introduction. The primary object of interest is the axial form factor. In the next section we show the details of this calculation.

---

[1] The derivatives are found using $\left.\frac{\partial\sigma}{\partial r}\right|_{r=L} = \frac{1}{2}\left.\frac{\partial\sigma}{\partial r}\right|_{r=L_-} + \frac{1}{2}\left.\frac{\partial\sigma}{\partial r}\right|_{r=L_+}$ and similarly for the pion field.

[2] As the case for $L = \infty$ is for all intents and purposes identical to the 100 fm case. We may then refer to the $L = 100$ fm case as the *infinite* volume solution, while $L = 3$ fm will be referred to as the *finite* volume solution.

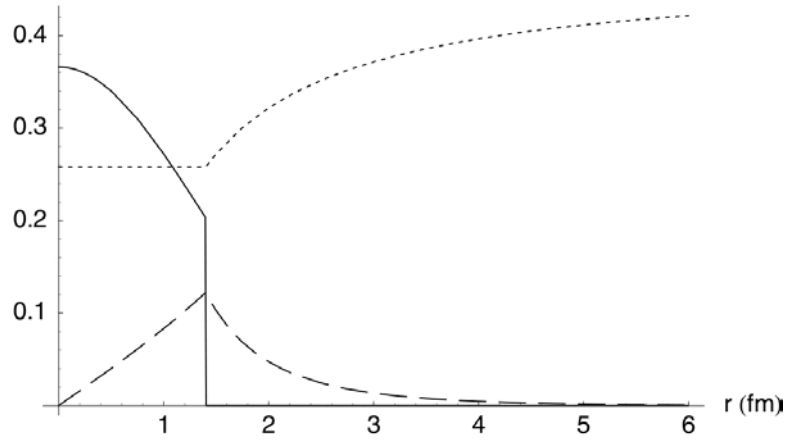

Figure 4.1: Fields for the infinite volume case: the solid line represents the quark fields, the dotted line the sigma field and the dashed line the pion fields respectively [TALY05].

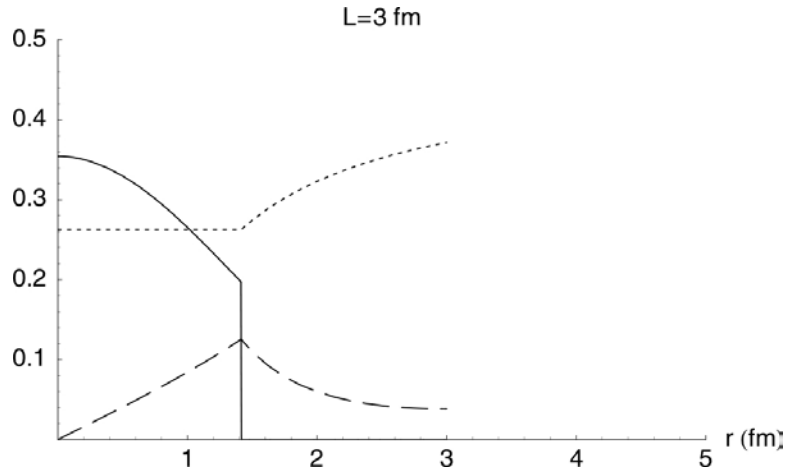

Figure 4.2: Fields for a finite volume case: the solid line represents the quark fields, the dotted line the sigma field and the dashed line the pion fields respectively [TALY05].

Figure 4.3: Kinematics of the reaction involving the axial current [PS].

4.2 The Axial Form Factor

The axial form factor provides information on the "spin-isospin distribution of the nucleon" [BEM02]. Before studying the specifics of the hedgehog's form factor calculation, there is a little more to be said about the general QCD form factor.

In QCD, the axial current is [PS],

$$A^\mu = \bar{Q}\gamma^\mu\gamma^5\tau^a Q \tag{4.34}$$

where,

$$Q = \begin{pmatrix} u \\ d \end{pmatrix} \tag{4.35}$$

Placing this between states we get the familiar factors shown in Eq. (2.32). Fig. 4.3 shows what happens kinematically. This is similar to what occurs with the hedgehog, except here the axial current is instead,

$$\vec{A}^\mu = \frac{1}{2}\bar{\psi}\gamma^\mu\gamma_5\vec{\tau}\psi\theta_{\rm R} + (\partial^\mu\sigma)\vec{\pi} - \sigma(\partial^\mu\vec{\pi})\,. \tag{4.36}$$

Substituting the expression for $\vec{A}^\mu$ into Eq. (2.32) gives,

$$\langle\,{\rm HH}\,|\vec{j}^{5a}(q)|\,{\rm HH}\,\rangle = \langle\,{\rm HH}\,|\int d^3r\, e^{i\vec{q}.\vec{r}}\frac{1}{2}\bar{\psi}\gamma^\mu\gamma_5\vec{\tau}\psi\theta_{\rm R} + (\partial^\mu\sigma)\vec{\pi} - \sigma(\partial^\mu\vec{\pi})|\,{\rm HH}\,\rangle$$

which will then give the axial form factor.

The most difficult part of taking the Fourier transform involves the quark field terms, i.e. $\frac{1}{2}\bar{\psi}\gamma^\mu\gamma^5\vec{\tau}\psi$. As we are looking at the static case, this term becomes $\frac{1}{2}\bar{\psi}\gamma^a\gamma^5\vec{\tau}\psi$, where $a = 1, 2, 3$. Substituting the field solutions

into Eqs. (4.10) and (4.11), the Fourier transform becomes,

$$\begin{aligned}\int d^3r e^{i\underline{q}\cdot\underline{r}}\frac{1}{2}\bar{\psi}(r)\gamma_a\gamma_5\vec{\tau}\psi(r) = \\ \int_0^R drr^2\int d\hat{r}e^{i\underline{q}\cdot\underline{r}}\frac{1}{2}\chi_h^\dagger\left(\alpha_+ j_0\left(\frac{\Omega r}{R}\right), -i\alpha_-\vec{\sigma}\cdot\hat{r}j_1\left(\frac{\Omega r}{R}\right)\right) \\ \cdot\gamma_0\gamma_5\gamma_a\vec{\tau}\begin{pmatrix}\alpha_+ j_0\left(\frac{\Omega r}{R}\right)\\ i\alpha_-\vec{\sigma}\cdot\hat{r}j_1\left(\frac{\Omega r}{R}\right)\end{pmatrix}\chi_h \\ = \int_0^R drr^2\frac{\chi_h^\dagger}{2}(\alpha_+^2 j_0^2\left(\frac{\Omega r}{R}\right) - \alpha_-^2 j_1^2\left(\frac{\Omega r}{R}\right))\left[\int d\hat{r}e^{i\underline{q}\cdot\underline{r}}\right]\sigma_a\vec{\tau}\chi_h \\ + \int_0^R drr^2\frac{\chi_h^\dagger}{2}2\alpha_-^2 j_1^2\left(\frac{\Omega r}{R}\right)\left[\int d\hat{r}e^{i\underline{q}\cdot\underline{r}}\vec{\sigma}\cdot\hat{r}\hat{r}_a\right]\vec{\tau}\chi_h \end{aligned} \tag{4.37}$$

where $d\hat{r}$ is the solid angle,

$$\int d\hat{r} = \int_0^\pi d\theta\sin\theta\int_0^{2\pi} d\phi\,. \tag{4.38}$$

Now we can choose a particular axis and, for simplicity's sake, we chose the 3-axis for both spin and isospin,

$$\begin{aligned}\text{R.H.S.} = \int_0^R drr^2\frac{\chi_h^\dagger}{2}(\alpha_+^2 j_0^2\left(\frac{\Omega r}{R}\right) - \alpha_-^2 j_1^2\left(\frac{\Omega r}{R}\right))\left[\int d\hat{r}e^{i\underline{q}\cdot\underline{r}}\right]\sigma_3\tau_3\chi_h \\ + \int_0^R drr^2\frac{\chi_h^\dagger}{2}2\alpha_-^2 j_1^2\left(\frac{\Omega r}{R}\right)\left[\int d\hat{r}e^{i\underline{q}\cdot\underline{r}}\vec{\sigma}\cdot\hat{r}\hat{r}_3\right]\tau_3\chi_h \end{aligned} \tag{4.39}$$

From Chodos and Thorn [CT75], we know that

$$\chi_h^\dagger\tau_i\sigma_j\chi_h = -\delta_{ij}\chi_h^\dagger\chi_h\,, \tag{4.40}$$

so the only non-zero term coming from the dot product in the second term is $\sigma_3\hat{r}_3$. This leaves us with the equation,

$$\begin{aligned}\int d^3r e^{i\underline{q}\cdot\underline{r}}\frac{1}{2}\bar{\psi}(r)i\gamma_3\gamma_5\tau_3\psi(r) = \\ \int_0^R drr^2\frac{\chi_h^\dagger}{2}(\alpha_+^2 j_0^2\left(\frac{\Omega r}{R}\right) - \alpha_-^2 j_1^2\left(\frac{\Omega r}{R}\right))\left[\int d\hat{r}e^{i\underline{q}\cdot\underline{r}}\right]\sigma_3\tau_3\chi_h \\ + \int_0^R drr^2\frac{\chi_h^\dagger}{2}2\alpha_-^2 j_1^2\left(\frac{\Omega r}{R}\right)\left[\int d\hat{r}e^{i\underline{q}\cdot\underline{r}}\hat{r}_3\hat{r}_3\right]\sigma_3\tau_3\chi_h \end{aligned} \tag{4.41}$$

After considerable work, the two integrals over the solid angles give,

$$\int d\hat{r} e^{i\underline{q}\cdot\underline{r}} = 4\pi j_0(qr); \tag{4.42}$$

$$\int d\hat{r} e^{i\underline{q}\cdot\underline{r}} \hat{r}_3 \hat{r}_3 = 4\pi(\frac{j_1(qr)}{qr} - j_2(qr)\hat{q}_3\hat{q}_3)\,, \tag{4.43}$$

while from Eq. (4.40),

$$\begin{aligned} \chi_h^\dagger \sigma_3\tau_3\chi_h &= -\chi_h^\dagger\chi_h \\ &= -N^2 \end{aligned} \tag{4.44}$$

where N is some normalisation constant and there will be a similar minus sign for $\langle\sigma_3\tau_3\rangle$ in a hedgehog elementary nucleon cancelling this one. Putting all this together our Fourier transform now becomes,

$$\begin{aligned} &\int d^3r e^{i\underline{q}\cdot\underline{r}} \frac{1}{2}\bar{\psi}(r) i\gamma_a\gamma_5\vec{\tau}\psi(r) = \\ &\quad 2\pi N^2 \int_0^R dr r^2 \Bigg\{ (\alpha_+^2 j_0^2\left(\frac{\Omega r}{R}\right) - \alpha_-^2 j_1^2\left(\frac{\Omega r}{R}\right)) j_0(qr) + 2\alpha_-^2 j_1^2\left(\frac{\Omega r}{R}\right) \\ &\qquad\qquad .(\frac{j_1(qr)}{qr} - j_2(qr)\hat{q}_3\hat{q}_3)\Bigg\} \end{aligned} \tag{4.45}$$

the last term in the integral involving the $\hat{q}_3\hat{q}_3$ is actually the quark contribution to the pseudoscalar form factor $G_P(q^2)$ and so we drop it here. The contributions from the sigma and pion fields can be worked out in a similar fashion, and when this is done, we get

$$\begin{aligned} G_{Ahh}\left(Q^2\right) &= 2\pi N^2 \int_0^R dr\, r^2 \Bigg\{ \left[\alpha_+^2 j_0^2\left(\frac{\Omega r}{R}\right) - \alpha_-^2 j_1^2\left(\frac{\Omega r}{R}\right)\right] j_0(qr) \\ &+ \alpha_-^2 2 j_1^2\left(\frac{\Omega r}{R}\right)\frac{j_1(qr)}{qr}\Bigg\} + 4\pi \int_0^\infty dr\, r^2 f'(r) g(r) \frac{j_1(qr)}{qr} \\ &- 4\pi \int_0^\infty dr\, r^2 f(r) \left[g'(r)\frac{j_1(qr)}{qr} + \frac{g(r)}{3r}\left(2j_0(qr) - j_2(qr)\right)\right] \end{aligned} \tag{4.46}$$

where the last two contributions are from the σ and $\vec{\pi}$ fields.

To compute the radius of the axial form factor we need $G_A(Q^2)/G(0)$ and must therefore find the expression for the axial charge g_A. We can do this by taking the limit $q \to 0$ in Eq. (4.46):

$$\begin{aligned} \lim_{q\to 0} j_0(qr) &= \lim_{q\to 0} \frac{\sin(qr)}{qr} \\ &= 1\,, \end{aligned}$$

and,

$$\begin{aligned} \lim_{q\to 0} \frac{j_1(qr)}{qr} &= \lim_{q\to 0} \left(\frac{\sin(qr)}{(qr)^3} - \frac{\cos(qr)}{(qr)^2} \right) \\ &= \frac{1}{3}\,, \end{aligned}$$

while the $\lim_{q\to 0} j_2(qr) = 0$. Thus our final expression for g_A is,

$$\begin{aligned} g_A &= 2\pi N^2 \int_0^R dr\, r^2 \Bigg\{ \left[\alpha_+^2 j_0^2\left(\frac{\Omega r}{R}\right) - \alpha_-^2 j_1^2\left(\frac{\Omega r}{R}\right) \right] + \alpha_-^2 \frac{2}{3} j_1^2\left(\frac{\Omega r}{R}\right) \Bigg\} \\ &\quad + \frac{4\pi}{3} \int_0^\infty dr\, r^2 f'(r) g(r) \\ &\quad - \frac{4\pi}{3} \int_0^\infty dr\, r^2 f(r) \left[g'(r) + \frac{2g(r)}{r} \right]. \end{aligned} \tag{4.47}$$

* * *

We now have an expression for $G_A(q^2)$ and all that remains is to evaluate the integral for several different values of L and m_π and observe how the axial form factor varies. On top that, the axial radius is derived from $G_A(q^2)$ so we can extend our working even further to see what volume dependence $\langle r_A^2 \rangle$ might have. This is done in the next section.

4.3 The Axial Radius

The mean square radius can be found from the slope of the form factor. In this case we are dealing with the axial radius and so needed to use Eq. (2.42). Here it is again,

$$\left\langle r_A^2 \right\rangle = -\frac{6}{G_A(0)} \frac{d}{dQ^2} G_A(Q^2) \Big|_{Q^2=0}\,, \tag{2.42}$$

where $Q^2 = -q^2$. As stated in chapter 2, the experimental axial form factor can be (well) approximated by a dipole of the form shown in Eq. (2.40).

$$G_A(Q^2) = g_A \left(\frac{1}{1 + \frac{Q^2}{\Lambda^2}} \right)^2 \tag{2.40}$$

Taking the derivative of the axial form factor,

$$\frac{d}{dQ^2} G_A(Q^2) = -2 \frac{g_A}{\Lambda^2}, \tag{4.48}$$

the axial radius becomes,

$$\left\langle r_A^2 \right\rangle = \frac{12}{\Lambda^2}, \tag{4.49}$$

where again Λ is the axial mass.

If we have only a small amount of data on $G_A(Q^2)$ at discrete values of Q^2, we must resort to cruder measures to approximate the slope of the form factor at $Q^2 = 0$, such as the ratio "rise over run" i.e.

$$\frac{d}{dQ^2} G_A(Q^2) = \frac{y_2 - y_1}{x_2 - x_1}, \tag{4.50}$$

where (x_1, y_1) and (x_2, y_2) are points on the graph $G_A(q^2)$. We use this second method to compare with lattice results because, as shown later on, near $q^2 = 0$ the model acts somewhat unexpectedly and the dipole form of Eq. (2.42) no longer applies. Because of the periodicity requirement,

$$q = \frac{2\pi}{d}, \tag{4.51}$$

the momentum q can only take certain integer multiples of $2\pi/L$. These values are reasonably spaced out and so this way of finding the slope at $Q^2 = 0$ is rather approximate. Nevertheless it still serves as an interesting comparison to the dipole option. Having said that, in the infinite volume situation, periodicity is no longer a requirement and so we can take a point as close to $Q^2 = 0$ as we want. In this particular circumstance the values for the dipole and the "rise over run" slope will be much closer.

* * *

Beginning with the Lagrangian and working with the Euler-Lagrange equations, we were able to explain how Refs. [TALY05] and [CT75] obtained the solutions in their respective scenarios. We explained how the non-linear

boundary condition along with the infinite volume solution for the σ field produced two eigenvalue equations from which we could extract the bag frequency and radius R. Using these values, along with the solutions for $\sigma(\vec{r})$ and $\vec{\pi}(\vec{r})$ in the axial current we performed a Fourier transform to work out the axial and pseudo-scalar form factors. This latter term was neglected as we were primarily interested in the $G_A(Q^2)$. From the physical dipole we showed how to find the mean square radius.

In the next chapter we present our results for the hedgehog axial form factor. By using multiple pion masses along with multiple volumes we seek to show what effect the finite volume of the lattice has on the form factor. Along with these results we also present our findings for the axial radius.

Chapter 5

Hedgehog Results

Before being able to calculate $G_A(Q^2)$ the eigenvalue problems,

$$4\pi R^4 B = \tau(\Omega, m_q, m_\pi, R, L) \tag{4.32}$$

$$f_\pi = f_0(R, \Omega) + a(R, \Omega)R\,, \tag{4.33}$$

needed to be solved. Initially this was done for $L \to \infty$, with eigenvalues of the lowest energy state chosen as this gave the shortest bag radius R. Using these values for R and Ω, the axial charge and axial form factor were calculated.

Once the infinite volume solutions were found, the eigenvalues for the *finite* volumes could be worked out. Table 5 shows these values for the case where the physical pion mass is used. Notice that the values converge to that for the $d = \infty$ solution. As pointed out in Refs. [TALY05] and [HTY] these values of R are rather large compared to the physical radius of ~ 0.8 fm[1].

[1]Since we are interested only in what happens when the boundary conditions are applied, the value of the radius is not really the issue.

d (fm)	Ω	R (fm)
5	1.60557	1.45501
6	1.58487	1.41483
10	1.58784	1.40043
20	1.58805	1.40000
∞	1.58805	1.40000

Table 5.1: Numerical solutions to the eigenvalue equations for $m_\pi = 140$ MeV.

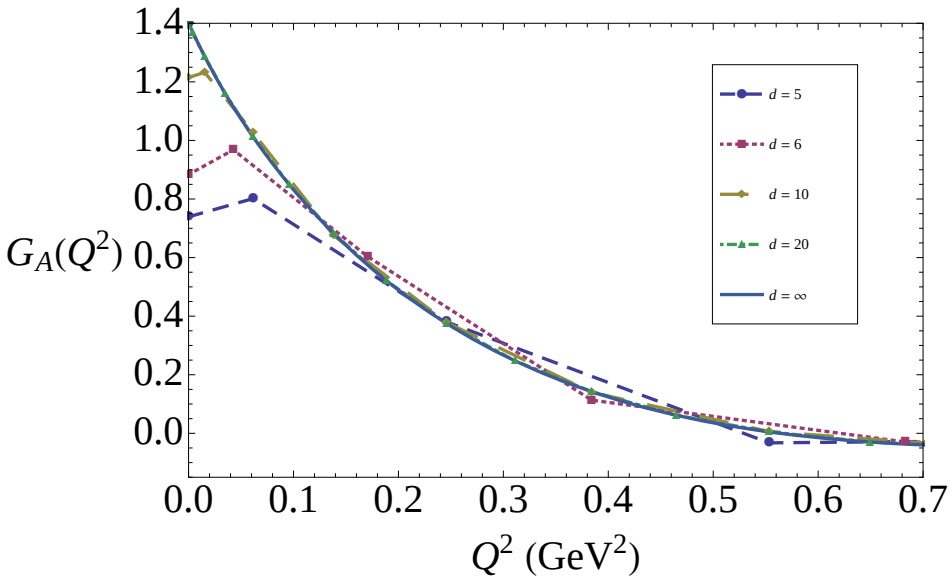

Figure 5.1: Axial form factor of the nucleon plotted versus Q^2 for a variety of diameters (d) of the lattice volume. The pion mass, m_π, is 140 MeV.

[TALY05].

Once these tasks were completed it was possible to find $G_A(Q^2)$. In the next section we show the results for three different pion masses over a range of volumes. After that the results for the axial radius are displayed.

5.1 $G_A(Q^2)$

Figure 5.1 shows the result for the physical pion mass, $m_\pi = 140$ MeV. At the moment lattice calculations of $G_A(Q^2)$ have not reached this value - the lowest calculations being performed are around the 270 MeV mark [Ale09] - so it is interesting to see what results lattice computations may find when they do reach the physical pion mass.

The eigenvalue equations for physical m_π could not be solved for some of the smaller d volumes. The lowest lattice diameter for which there were solutions was $d = 5$, corresponding to a gap of around 1.1 fm between the bag surface and lattice edge. For the other pion masses, 300 and 500 MeV, solutions were possible down to $d = 3.6$ fm with a gap between the bag surface and lattice edge of ~ 0.4 fm.

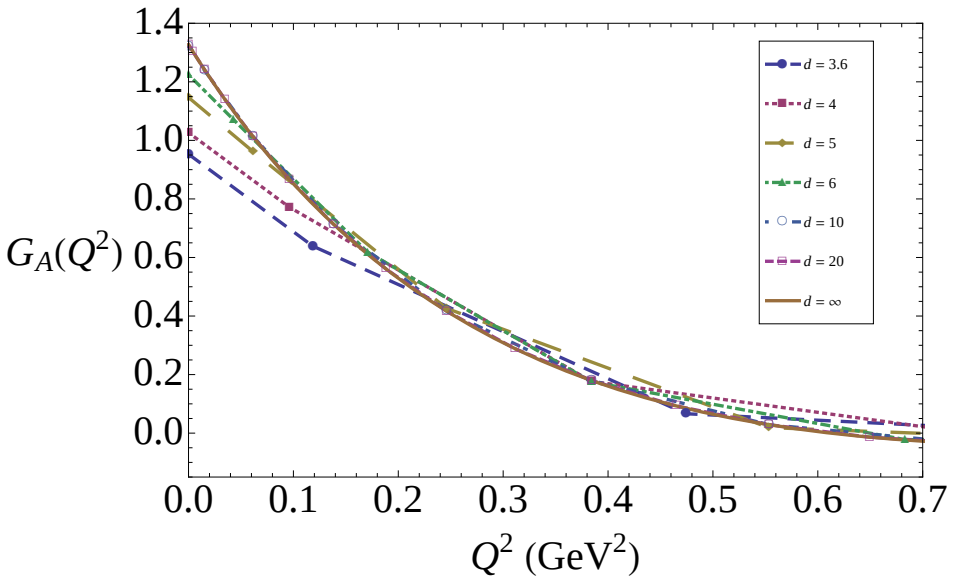

Figure 5.2: Axial form factor of the nucleon plotted versus Q^2 for a variety of diameters (d) of the lattice volume. The pion mass, m_π, is 300 MeV.

In the physical pion case there is clearly a large volume dependence: the axial form factor becomes flatter and flatter as the volume decreases. Notice that it also turns over for small Q^2 [HTY]. Although this particular feature makes a fit with a simple dipole impossible as it produces a negative axial radius, it does not take away from the fact that there are significant changes to the $G_A(Q^2)$ as the volume gets smaller.

Fig. 5.2 shows the $m_\pi = 300$ MeV case. This value is much closer to the graph in Ref. [B$^+$10] where the pion mass was 356 MeV. Notice that the form factor no longer turns over for small Q^2 as in the previous graph. As before there is a strong, albeit smaller, volume dependence. For $d = 3.6$ fm the curve is much much lower than the $d = 20$ case - which is almost identical to the infinite volume solution.

Finally, the much larger π mass is given in Fig. 5.3. In this result there is very little volume dependence. All the curves are closely bunched up together for the entire range of Q^2, with only a very small difference between smallest volume and the infinite volume. This tells us that the volume dependence of the axial form factor disappears with increasing m_π.

It is clear from all these figures that for our model the axial form factor has a large volume dependence for the range of pion masses that Bratt *et al.* were using. For both the 140 MeV and 300 MeV cases the form factor became

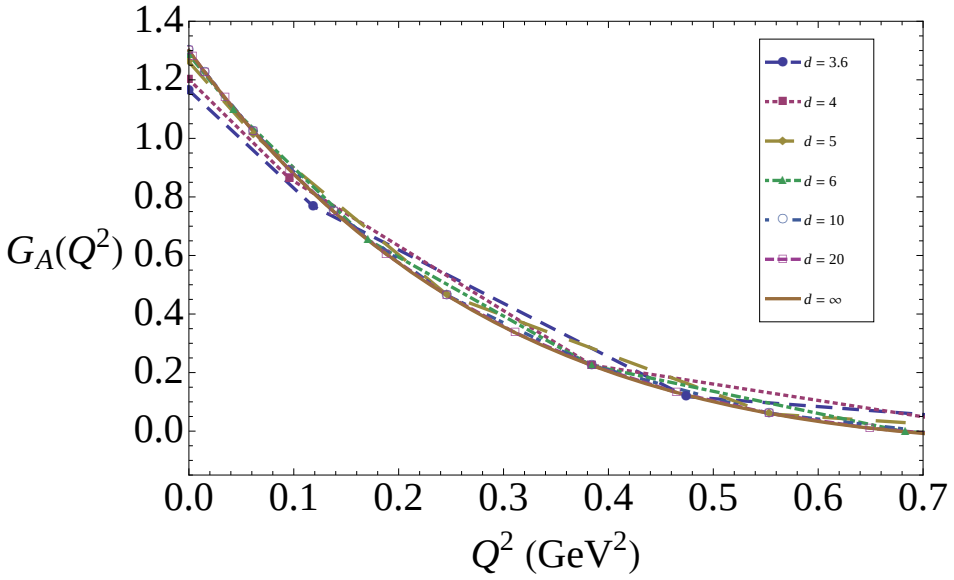

Figure 5.3: Axial form factor of the nucleon plotted versus Q^2 for a variety of diameters (d) of the lattice volume. The pion mass, m_π, is 500 MeV.

significantly flatter as the lattice volume decreased. Therefore, although it is not possible to say conclusively, these results suggest that it is large finite volume effects which are lowering the lattice values.

In the previous chapter we looked at the graphs of the quark, sigma and pion fields for the both the finite (Fig. 4.2) and infinite (Fig. 4.1) volumes. Comparing these two graphs we saw that both the quark and sigma fields showed little change. However, the pion field was much larger for $L = 3$ than for the infinite case and this was suggested to be caused by the fact that the pion field did not have enough time to die off before reaching the edge of the lattice. It would therefore be interesting to see if the behaviour of the fields is mirrored by their individual contributions to $G_A(Q^2)$. The specific contributions made by each field to the axial form factor are shown in Figs. 5.4 - 5.6. In each case $m_\pi = 300$ MeV.

The graphs for the quark and sigma field show very little change over the entire range of volumes. The quark fields are extremely similar for small momentum transfer and then slowly separate for larger Q^2. On the other hand, the sigma field is virtually identical for all values of Q. These results suggest that no significant volume dependence is coming from either of these fields. However, the situation is very different for the pion field, Fig. 5.6 shows a large difference between curves for varying volumes. These three

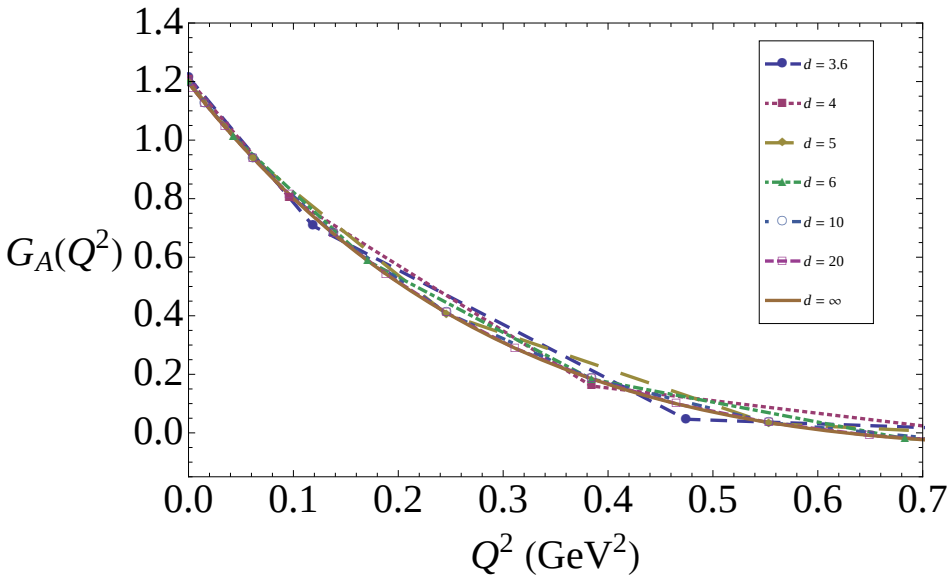

Figure 5.4: Quark field contribution to the axial form factor for $m_\pi = 300$ MeV.

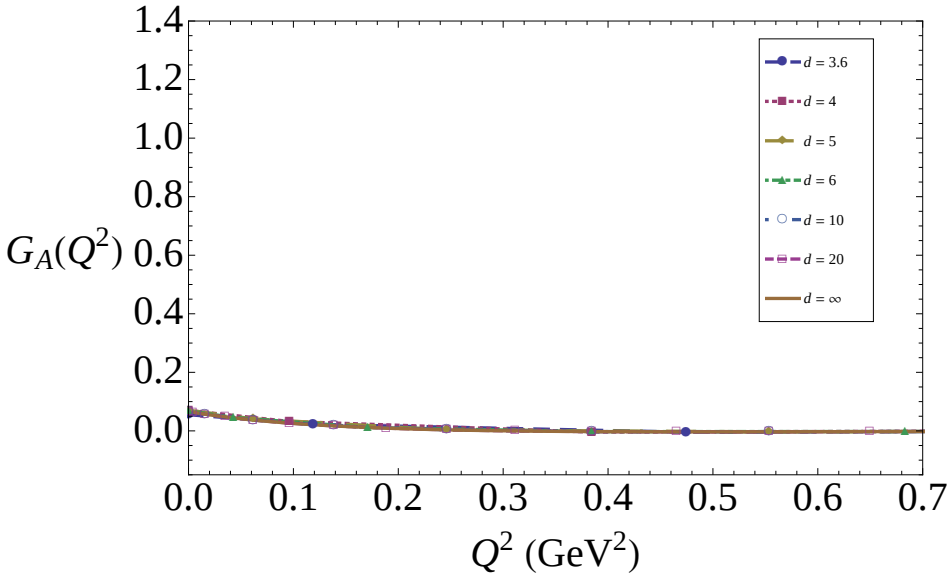

Figure 5.5: Sigma field contribution to the axial form factor for $m_\pi = 300$ MeV.

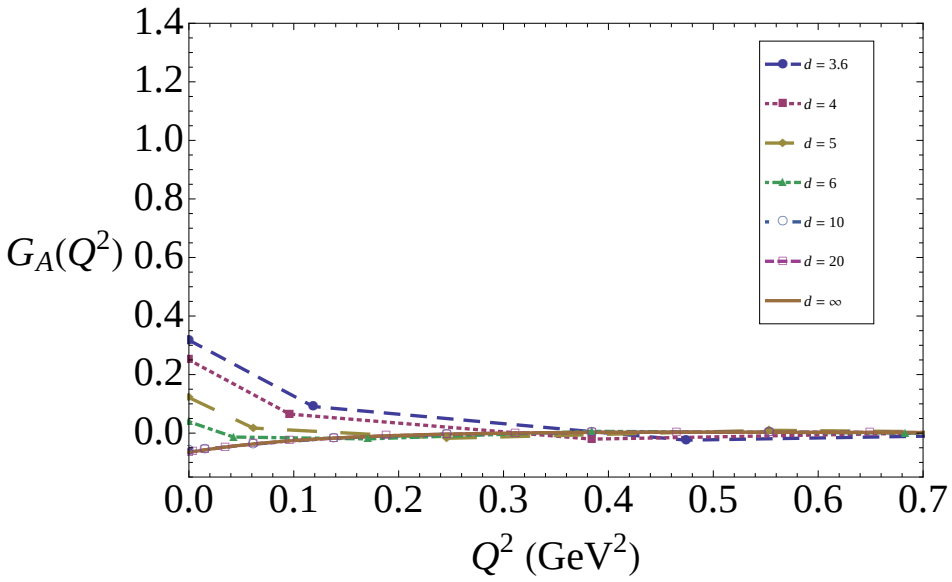

Figure 5.6: Pion field contribution to the axial form factor for $m_\pi = 300$ MeV.

graphs do indeed mirror our results from chapter 2 and also confirm our suspicion that the finite volume effects in this model were due to the pion field.

Alternate Boundary Conditions

In the previous chapter we also discussed the use of a different boundary condition for the pion field. Setting the pion field to be zero at the edge of the lattice instead of the gradient, we found that resulting solution for the pion field was somewhat altered. As Figs. 5.7 and 5.8 show, the axial form factors have also been affected, no longer showing any volume dependence at low Q^2. These figures show quite clearly that the model's volume dependence relies on setting the gradient to zero at the boundary. Although these results are interesting to look at, we follow Ref. [TALY05] in saying that it is the original boundary conditions which represent the lattice periodic conditions.

The results for the hedgehog's axial form factor have now been shown in detail. We can now, therefore, turn to the axial radius, where once again we use the original boundary conditions for the pion field. Given the relationship between the two observables - Eq. (2.42) - we know there must be similar finite volume effects for the axial radius also.

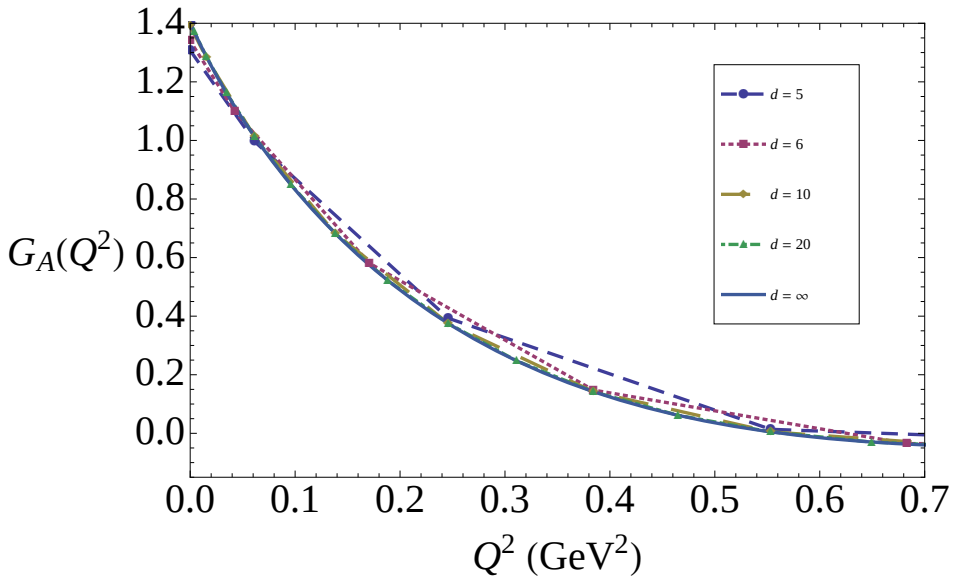

Figure 5.7: Axial form factor of the nucleon plotted versus Q^2 for a variety of diameters (d) of the lattice volume with new boundary conditions. The pion mass, m_π, is 140 MeV.

5.2 $\langle r_A^2 \rangle$

In the earlier discussion of the axial radius we mentioned that it was possible to find the slope of G_A, and thus $\langle r_A^2 \rangle$, in different ways. The conventional way is to use the Eq. (2.40) for the physical dipole and take its derivative. These results for the pion mass of 300 MeV are shown in Table. 5.2. The other approach is to use the "rise over run" method. Figs. 5.9 - 5.11 show the comparison between these two methods.

In the first graph, the two curves are almost identical, with the axial radius demonstrating strong volume dependence, slowly converging to the infinite volume value. Note also that for small volumes the axial radius is negative. This is expected because of the shape of the form factor.

The case where the π mass is 300 MeV also has evidence of finite volume effects. Importantly though, there are no negative radii - thus corresponding much more closely to the physical $\langle r_A^2 \rangle$. There is now a discernible difference between dipole and "slope" graphs but their shape is still essentially the

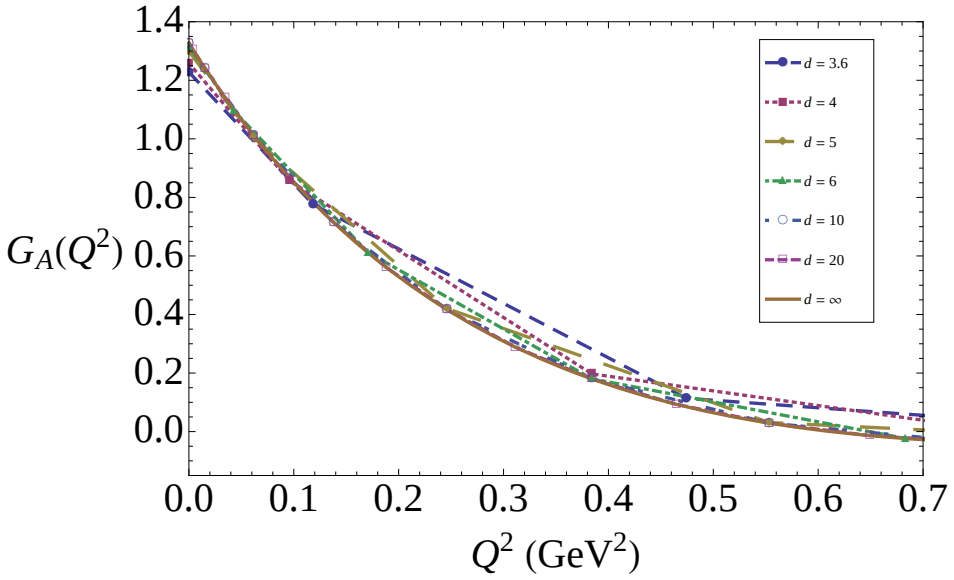

Figure 5.8: Axial form factor of the nucleon plotted versus Q^2 for a variety of diameters (d) of the lattice volume with new boundary conditions. The pion mass, m_π, is 300 MeV.

d (fm)	$\langle r_A^2 \rangle$ (fm)	Λ^2 (GeV)
5	0.69746	0.818387
6	0.75503	0.786568
10	0.97325	0.692796
20	1.02556	0.674897
∞	1.02207	0.676049

Table 5.2: Results for the axial radius and axial mass with $m_\pi = 300$ MeV.

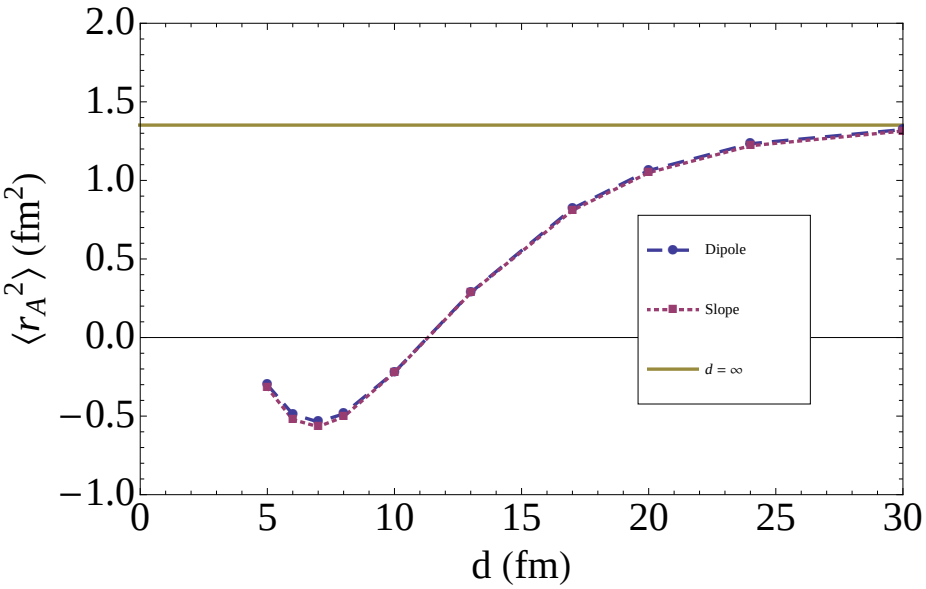

Figure 5.9: Axial radius of the nucleon versus the diameter of the lattice volume d for $m_\pi = 140$ MeV.

same. However in order to compare with Bratt *et al.* it is perhaps best to use the dipole, given this is what they used for their results.

Finally, for Fig. 5.11 there is very little volume dependence. This agrees with what we saw for G_A at this mass. What is interesting though is that while the dipole r_A hugs the infinite volume value, showing virtually no difference, using the "rise over run" ratio for the slope showed a discernibly larger volume dependence - reaching the $d = \infty$ value really only for a diameter of 13 fm.

Combining the graphs for the dipole into a plot (Fig. 5.12) of the axial radius against the pion mass squared makes the volume dependence even more explicit. It is interesting to note that even for large diameters - exceptionally large in fact, when compared with the lattices currently in use - the axial radius is notably smaller than the infinite volume for small m_π.

* * *

The results for the hedgehog axial form factor have now been shown in detail. A comparison of Figs. 5.1 to 5.3 provides compelling evidence of G_A being flattened by finite volume effects. These effects are seen most clearly in the $m_\pi = 300$ MeV case, with the 140 MeV case suffering from

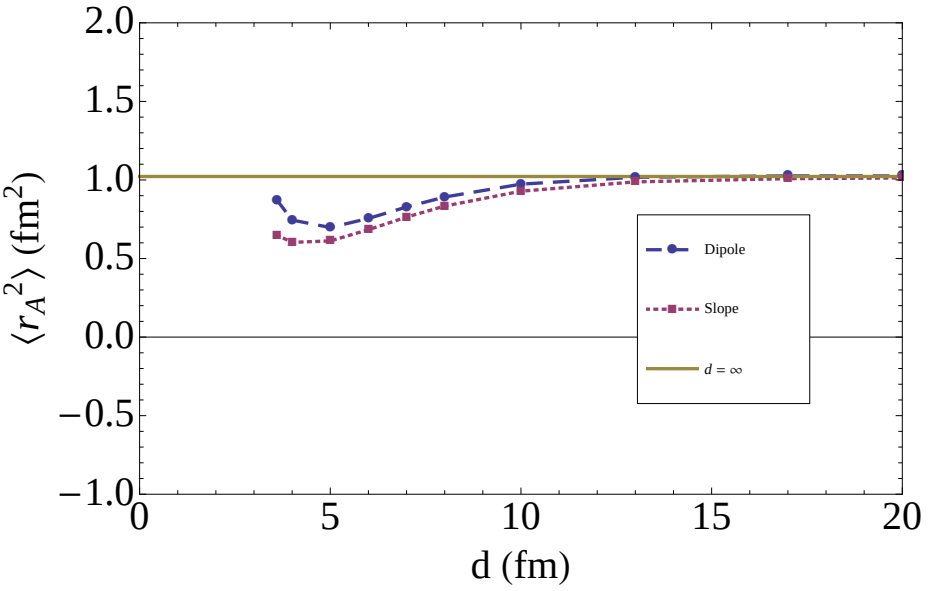

Figure 5.10: Axial radius of the nucleon versus the diameter of the lattice volume d for $m_\pi = 300$ MeV.

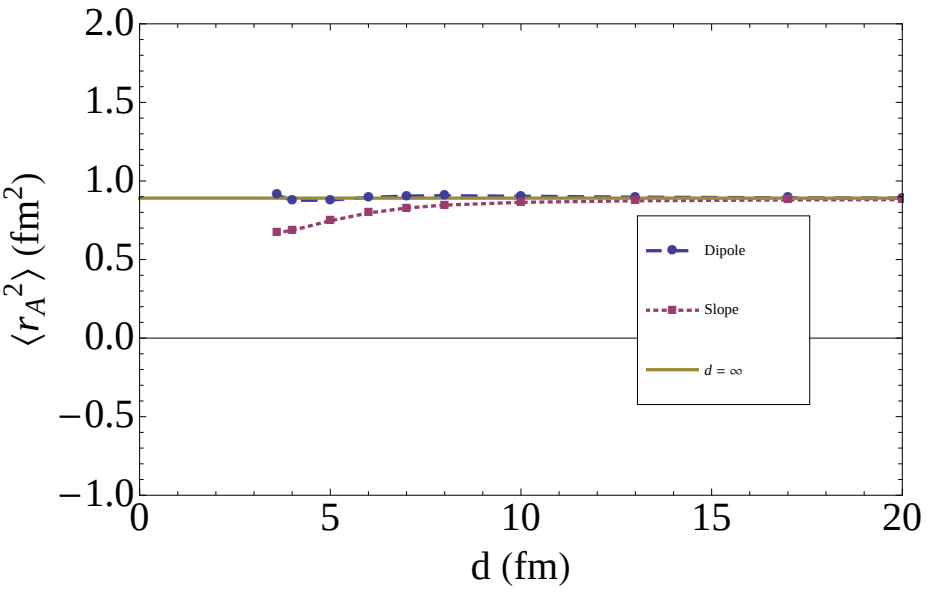

Figure 5.11: Axial radius of the nucleon versus the diameter of the lattice volume d for $m_\pi = 500$ MeV.

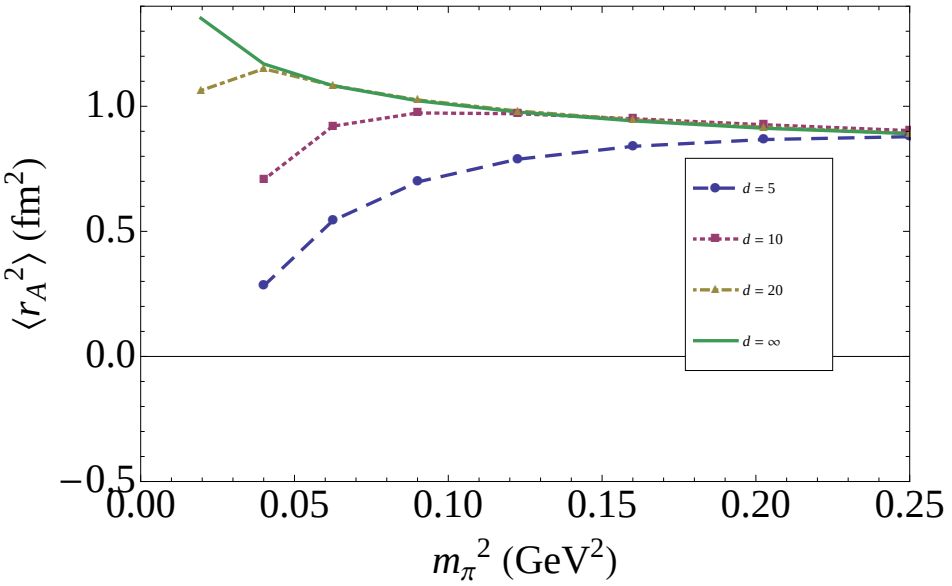

Figure 5.12: Axial radius of the nucleon versus pion mass for several different lattice volumes, including the infinite volume case.

some unphysical issues, while there were only small volumes effects at 500 MeV.

By looking at each field's individual contribution, we found that the finite volume effects were due to the pion field with quark and sigma fields showing very little variation over the range of diameters used. This is what was suspected in chapter 2 after comparing the graphs of the finite and infinite volume solutions.

We also looked at the axial radius and saw that these results exhibited a similar volume dependence.

Chapter 6

Corrections Involving Nucleon Spin-flip

In the past few chapters we have looked at the hedgehog model and the finite volume effects on its axial form factor. We saw that this effect was quite large, given the right boundary conditions. However this particular set up, although similar, is not directly related to the situation on the lattice, and hence it is difficult to show that finite volume effects are the cause of the discrepancy between experimental and lattice values. Indeed, Cohen [Coh02] argues that the finite volume effects on the pion pole cannot be the cause of small values of g_A and if this is the case, then neither would $G_A(Q^2)$ be effected.

In an attempt to find an alternative explanation we now look at what happens in the case where the situation more closely resembles the conditions on the lattice. Calculations of one-loop finite volume corrections have already been made by Beane and Savage [BS04] and Detmold and Lin [DL05] for the nucleon axial form factor, and to these we add another correction.

For the case where the nucleons are considered point-like we calculate corrections involving the tensor interaction which arise from the fact that periodic boundary conditions mean that each nucleon is surrounded by a neighbouring set of nucleons. This approximation is valid when the lattice containing the nucleon is much larger than the nucleon. At this point it is important to note that we will now be dealing with the conventional four-dimensional box and *not* the spherical cavity that was used earlier; as a result L is now the side length and not the radius.

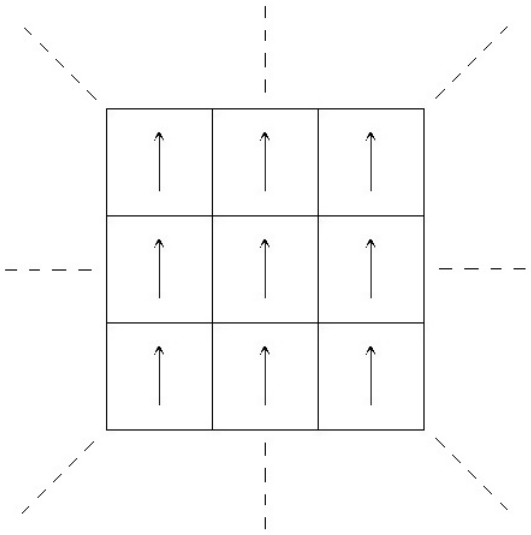

Figure 6.1: Lattice nucleon with spin up surrounded by neighbouring nucleons.

6.1 Point-like Nucleon

For large L, the nucleon can be thought of as a point-like particle. Fig. [6.1] shows a two-dimensional view of what the situation looks like when the standard boundary conditions are applied. As shown, each nucleon is surrounded by other nucleons. These are a direct consequence of periodic/anti-periodic boundary conditions[1].

In chapter 3 we mentioned that in the CBM the quarks are confined to a spherical bag with pion fields being allowed to move inside and outside the bag thus bringing to mind the picture of a "cloud" of pions. Now at any point in time, there is the possibility that one of the nucleons will emit a pion which is then absorbed by one of the surrounding nucleons. In the case where the pion emitted is a π^0, the proton, say, which emits this pion will most likely have its spin flipped. The neighbouring proton which absorbs the π^0 is also most likely to have its spin flipped[2]. This reaction is shown in Fig. 6.2 with time going up the page.

This spin flip that occurs has the effect of lowering the axial charge

[1] In actual fact there are surrounding nucleons in one other dimension bringing the *direct* neighbour count to 6.

[2] This process cannot occur for $\pi^{\pm}$ since conservation of charge would prevent the proton from remaining a proton and we may, for example, end up with particles of different charge in neighbouring boxes thus destroying the periodicity requirement.

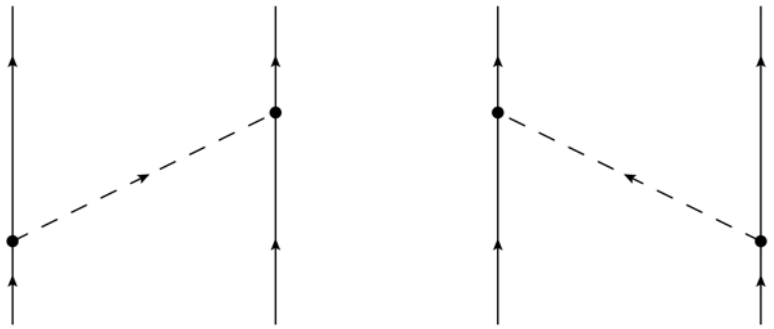

Figure 6.2: Proton emitting a π^0 before it being absorbed by a neighbouring proton.

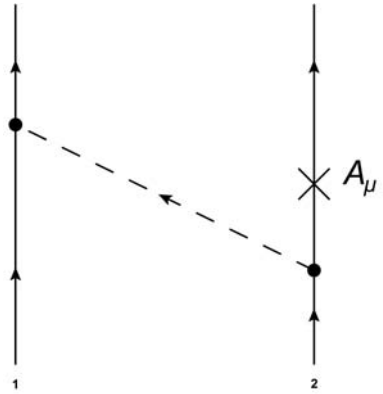

Figure 6.3: Proton emitting/absorbing a π^0 with the axial current inserted.

g_A which in turn will lower the axial form factor. Fig. 6.3 shows the same process, except now an axial current is inserted in order to measure g_A.

We now examine the magnitude of the change in the axial charge and whether it is large enough to account for the discrepancy seen in lattice simulations.

Calculation

The amplitude for the reaction (in this case going from spin down to spin up) shown on the right-hand side of Fig 6.3 looks like,

$$\begin{aligned}\left\langle p_1\uparrow p_2\uparrow|H_{\rm int}\,|\,p_1\downarrow p_2\uparrow\pi^0_{\underline{k}}\right\rangle G_0 \\ \times\left\langle p_1\downarrow p_2\uparrow\pi^0_{\underline{k}}\,|\,A_{2z}\,|\,p_1\downarrow p_2\uparrow\pi^0_{\underline{k}}\right\rangle G_0 \\ \times\left\langle p_1\downarrow p_2\uparrow\pi^0_{\underline{k}}\,|\,H_{\rm int}\,|\,p_1\downarrow p_2\downarrow\right\rangle\end{aligned} \tag{6.1}$$

where,

$$\begin{aligned}\left\langle p_1\uparrow p_2\uparrow|H_{\rm int}\,|\,p_1\downarrow p_2\uparrow\pi^0_{\underline{k}}\right\rangle &= \langle p_1\uparrow\,|\,H_{\rm int}\,|\,p_1\downarrow\pi^0_{\underline{k}}\rangle \\ &= i\sqrt{\frac{2\pi}{\omega_k}}\frac{f_{NN\pi}}{m_\pi}v_k\tau_{13}\langle\chi_{1/2}\,|\,\vec\sigma_1\cdot\vec k\,|\,\chi_{-1/2}\rangle\,,\end{aligned} \tag{6.2}$$

and,

$$\begin{aligned}\left\langle p_1\downarrow p_2\uparrow\pi^0_{\underline{k}}\,|\,H_{\rm int}\,|\,p_1\downarrow p_2\downarrow\right\rangle &= \langle p_2\uparrow\pi^0_{\underline{k}}\,|\,H_{\rm int}\,|\,p_2\downarrow\rangle \\ &= (-i)\sqrt{\frac{2\pi}{\omega_k}}\frac{f_{NN\pi}}{m_\pi}v_k\tau_{23}\langle\chi_{1/2}\,|\,\vec\sigma_2\cdot\vec k\,|\,\chi_{-1/2}\rangle\,,\end{aligned} \tag{6.3}$$

while $\left\langle p_1\downarrow p_2\uparrow\pi^0_{\underline{k}}\,|\,A_{2z}\,|\,p_1\downarrow p_2\uparrow\pi^0_{\underline{k}}\right\rangle$ is what we calculated in the previous chapter. $G_0 = 1/\omega_k$ is the propagator and v_k is the phenomenological function which for now we set to one[3]. Since only the π^0 is involved in this interaction, only the τ_{i3} component is included in the amplitude.

Substituting Eqs. (6.2) and (6.3) into Eq. (6.1) and then taking the Fourier transform we have,

$$\begin{aligned}&\langle A_{2z}\rangle\left\langle\frac12\,\frac12\right|\int\frac{d^3k}{(2\pi)^3}\,e^{i\vec k\cdot\vec L} \\ &\qquad .(-i^2)\,\frac{2\pi}{\omega_k}\,\left(\frac{f_{NN\pi}}{m_\pi}\right)^2(v_k)^2\,\tau_{13}\,\vec\sigma_1\cdot\vec k\,\frac{1}{(\omega_k)^2}\,\tau_{23}\,\vec\sigma_2\cdot\vec k\,\left|-\frac12\;-\frac12\right\rangle \\ &= \langle A_{2z}\rangle\left\langle\frac12\,\frac12\right|\frac{\tau_{13}\tau_{23}}{(2\pi)^2}\left(\frac{f_{NN\pi}}{m_\pi}\right)^2\int d^3k\,e^{i\vec k\cdot\vec L}\,(v_k)^2\,\frac{\vec\sigma_1\cdot\vec k\,\vec\sigma_2\cdot\vec k}{(k^2+m_\pi^2)^{3/2}}\left|-\frac12\;-\frac12\right\rangle.\end{aligned} \tag{6.4}$$

[3]Later, when we look at the bag-like nucleon, v_k is no longer equal to one.

Setting $v_k = 1$ and since we know that

$$\vec{k}e^{i\vec{k}\cdot\vec{L}} = \frac{\vec{\nabla}}{i}e^{i\vec{k}\cdot\vec{L}}\,, \tag{6.5}$$

for $\vec{\nabla} = \partial/\partial\vec{L}$, this becomes,

$$\begin{aligned} &= \langle A_{2z}\rangle\left\langle \frac{1}{2}\,\frac{1}{2}\right| \frac{\tau_{13}\tau_{23}}{(2\pi)^2}\left(\frac{f_{NN\pi}}{m_\pi}\right)^2 \vec{\sigma}_1\cdot\frac{\nabla}{i}\vec{\sigma}_2\cdot\frac{\nabla}{i}\int d^3k\frac{e^{i\vec{k}\cdot\vec{L}}}{(k^2+m_\pi^2)^{3/2}}\left| -\frac{1}{2}\ -\frac{1}{2}\right\rangle \\ &= \langle A_{2z}\rangle\left\langle \frac{1}{2}\,\frac{1}{2}\right| \frac{\tau_{13}\tau_{23}}{(2\pi)^2}\left(\frac{f_{NN\pi}}{m_\pi}\right)^2 \vec{\sigma}_1\cdot\frac{\nabla}{i}\vec{\sigma}_2\cdot\frac{\nabla}{i}\int_0^\infty dk\frac{k^2}{(k^2+m_\pi^2)^{3/2}} \\ &\qquad\qquad .\int d\hat{k}e^{i\vec{k}\cdot\vec{L}}\left| -\frac{1}{2}\ -\frac{1}{2}\right\rangle. \end{aligned}$$

However, as we found earlier, (Eq. (4.42)),

$$\int d\hat{k}e^{i\vec{k}\cdot\vec{L}} = 4\pi j_0(kL); \tag{4.42}$$

so the amplitude becomes,

$$\begin{aligned} &\langle A_{2z}\rangle\left\langle \frac{1}{2}\,\frac{1}{2}\right| \frac{\tau_{13}\tau_{23}}{(2\pi)^2}\left(\frac{f_{NN\pi}}{m_\pi}\right)^2 \vec{\sigma}_1\cdot\frac{\nabla}{i}\vec{\sigma}_2\cdot\frac{\nabla}{i}\int_0^\infty dk\frac{k^2}{(k^2+m_\pi^2)^{3/2}} \\ &\qquad\qquad .4\pi\, j_0(kL)\left| -\frac{1}{2}\ -\frac{1}{2}\right\rangle. \end{aligned} \tag{6.6}$$

Performing the momentum integral we have:

$$\int_0^\infty dk\frac{k^2}{(k^2+m_\pi^2)^{3/2}}\, j_0(kL) = K_0(m_\pi L)\,, \tag{6.7}$$

where $K_0(m_\pi L)$ is the modified Bessel function. Substituting this result into Eq. (6.6) the amplitude ends up as,

$$\begin{aligned} &\langle A_{2z}\rangle\left\langle \frac{1}{2}\,\frac{1}{2}\right| \frac{\tau_{13}\tau_{23}}{(2\pi)^2}\left(\frac{f_{NN\pi}}{m_\pi}\right)^2 \vec{\sigma}_1\cdot\frac{\nabla}{i}\vec{\sigma}_2\cdot\frac{\nabla}{i}\int_0^\infty dk\frac{k^2}{(k^2+m_\pi^2)^{3/2}} \\ &\qquad\qquad .4\pi\, j_0(kL)\left| -\frac{1}{2}\ -\frac{1}{2}\right\rangle \\ &= \langle A_{2z}\rangle\left\langle \frac{1}{2}\,\frac{1}{2}\right| \frac{\tau_{13}\tau_{23}}{(2\pi)^2}\left(\frac{f_{NN\pi}}{m_\pi}\right)^2 \vec{\sigma}_1\cdot\frac{\nabla}{i}\vec{\sigma}_2\cdot\frac{\nabla}{i}\,4\pi\, K_0(m_\pi L)\left| -\frac{1}{2}\ -\frac{1}{2}\right\rangle. \end{aligned} \tag{6.8}$$

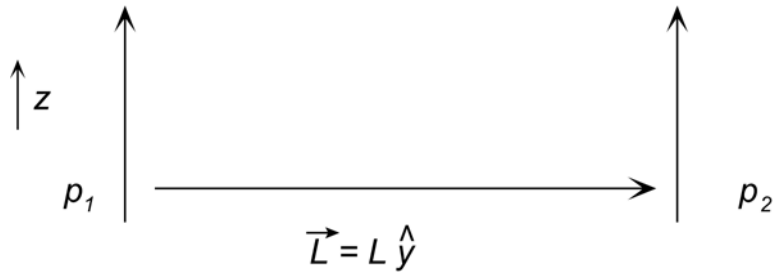

Figure 6.4: Two nucleons with spin up a distance L apart.

In this reaction the spins of the protons are being flipped from down to up, which means that the only component from $\vec{\sigma}_i \cdot \nabla$ to contribute to this amplitude is σ_{i+} since,

$$\begin{aligned} \langle 1/2 \,|\, \sigma_+ |\, -1/2 \rangle &= \langle 1/2 \,|\, 1/2 \rangle \\ &= 1 \end{aligned} \tag{6.9}$$

where the i index refers to the particular proton involved. If,

$$\sigma_{i\pm} = \mp \frac{1}{2}(\sigma_{ix} \pm i\sigma_{iy}); \qquad \sigma_{i0} = \sigma_{iz}, \tag{6.10}$$

and similarly,

$$\nabla_\pm = \mp \frac{1}{2}(\nabla_x \pm i\nabla_y); \qquad \nabla_0 = \nabla_z, \tag{6.11}$$

then

$$\vec{\sigma}_i \cdot \nabla = -2(\sigma_{i-}\nabla_+ + \sigma_{i+}\nabla_-) + \sigma_{i0}\nabla_0. \tag{6.12}$$

Since only the σ_{i+} terms contribute, we can substitute $\sigma_{i+}\nabla_-$ for $\vec{\sigma}_i \cdot \nabla$ in Eq. (6.8). Then, given that the interaction is proportional to dot product of $\sigma_{i\pm}$ and L, it is clear from Fig. 6.4 that the $\nabla_- = \frac{1}{2}(\nabla_x - i\nabla_y)$ term will be greatest when $\nabla_y = \partial/\partial L$. Including these extra modifications we have

$$\begin{aligned}
&\langle A_{2z}\rangle\left\langle \frac{1}{2}\,\frac{1}{2}\right| \frac{\tau_{13}\tau_{23}}{(2\pi)^2}\left(\frac{f_{NN\pi}}{m_\pi}\right)^2 \vec{\sigma}_1\cdot\frac{\nabla}{i}\vec{\sigma}_2\cdot\frac{\nabla}{i}\,4\pi\,K_0(m_\pi L)\left|-\frac{1}{2}\;-\frac{1}{2}\right\rangle \\
&= \langle A_{2z}\rangle\left\langle \frac{1}{2}\,\frac{1}{2}\right| \frac{\tau_{13}\tau_{23}}{(2\pi)^2}\left(\frac{f_{NN\pi}}{m_\pi}\right)^2 \frac{4\pi}{i^2}\,4\,(\sigma_{1+}\nabla_-)(\sigma_{2+}\nabla_-)\,K_0(m_\pi L)\left|-\frac{1}{2}\;-\frac{1}{2}\right\rangle \\
&= \langle A_{2z}\rangle\left\langle \frac{1}{2}\,\frac{1}{2}\right| \frac{\tau_{13}\tau_{23}}{(2\pi)^2}\left(\frac{f_{NN\pi}}{m_\pi}\right)^2 \frac{4\pi}{i^2}\,4\,\sigma_{1+}(-\frac{i}{2}\frac{\partial}{\partial L})\sigma_{2+}(-\frac{i}{2}\frac{\partial}{\partial L}) \\
&\qquad\qquad .K_0(m_\pi L)\left|-\frac{1}{2}\;-\frac{1}{2}\right\rangle \\
&= \langle A_{2z}\rangle\left\langle \frac{1}{2}\,\frac{1}{2}\right| \frac{\tau_{13}\tau_{23}}{(2\pi)^2}\left(\frac{f_{NN\pi}}{m_\pi}\right)^2 4\pi\frac{4}{i^2}\,\frac{i^2}{4}\,\sigma_{1+}\sigma_{2+}\frac{\partial^2}{\partial L^2}\,K_0(m_\pi L)\left|-\frac{1}{2}\;-\frac{1}{2}\right\rangle .
\end{aligned} \tag{6.13}$$

Differentiating the Bessel K function,

$$\frac{\partial^2}{\partial L^2}K_0(m_\pi L) = \frac{1}{2}m_\pi^2(K_0(m_\pi L) + K_2(m_\pi L)), \tag{6.14}$$

and substituting in,

$$4\pi\left(\frac{f_{NN\pi}}{m_\pi}\right)^2 = \left(\frac{g_A}{2f_\pi}\right)^2; \tag{6.15}$$

the final form of the amplitude is:

$$\langle A_{2z}\rangle\left\langle \frac{1}{2}\,\frac{1}{2}\right| \frac{\tau_{13}\tau_{23}}{(2\pi)^2}\left(\frac{g_A}{2f_\pi}\right)^2\sigma_{1+}\sigma_{2+}\frac{m_\pi^2}{2}\,[K_0(m_\pi L) + K_2(m_\pi L)]\left|-\frac{1}{2}\;-\frac{1}{2}\right\rangle . \tag{6.16}$$

A plot of this function, not including the $\langle A_{2z}\rangle$ part of course, and for physical pion mass is shown in Fig. 6.5. This graph shows us that at the lattice size of $L = 2$ fm the correction to the form factor is ~ 1 % multiplying this by 4 to include the other nearest neighbour protons, the total moves up to roughly 4 % for physical m_π. Corrections from other neighbours can be included as well. If we look at Fig. 6.6, then the light gray shows the neighbouring protons which have already been included. The boxes labelled "N" are the next largest contributors, with $L \to \sqrt{2}L$ since the distance between them and the original proton is $\sqrt{2}L$, there are four of these. The eight protons labelled "M" are similar to the previous one except now there is a factor of 1/2 out the front as well. Finally, the smallest contributors, "J", as well as including the 1/2 factor out the front, have $L \to \sqrt{3}L$. Adding up all these additional terms brings the total correction to about 8.4 %. While, in itself, this is not sufficient to explain the full suppression seen in lattice QCD it is a substantial correction.

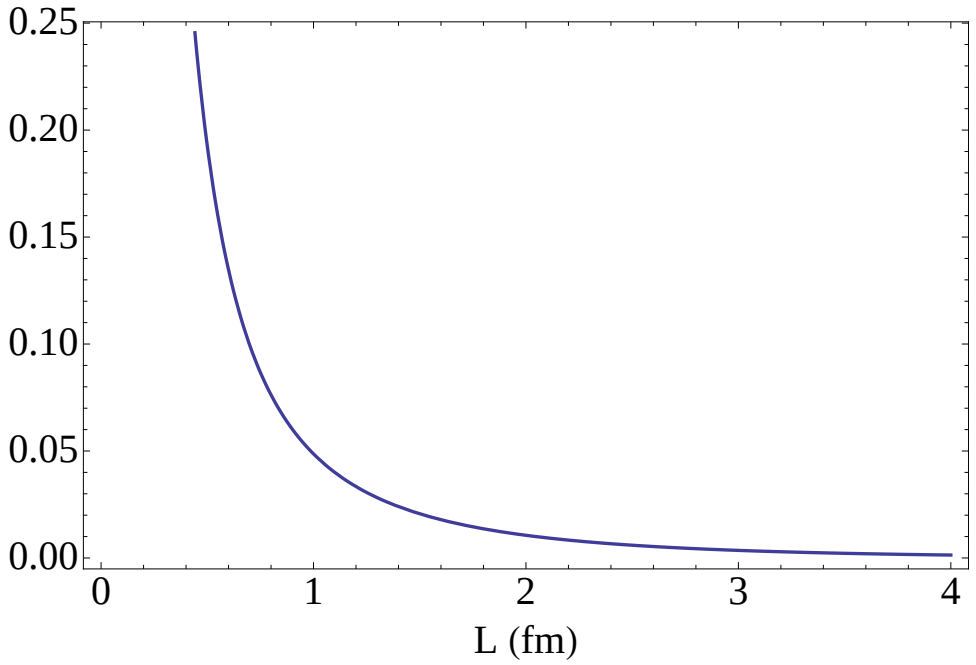

Figure 6.5: Correction to the axial form factor as a result of proton interactions via the π^0.

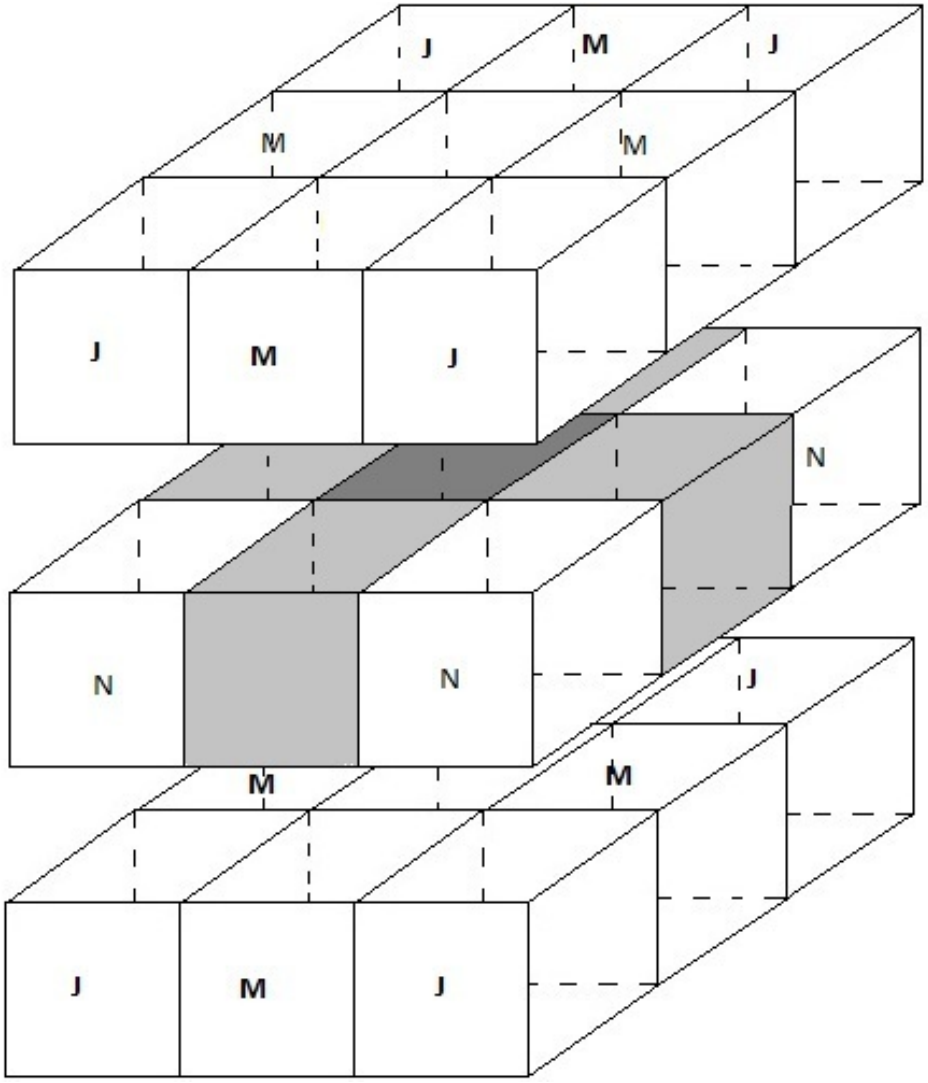

Figure 6.6: Static lattice box with surrounding nucleons.

Chapter 7

Conclusion

Lattice QCD has been extremely successful over the course of its lifetime. New techniques, coupled with ever increasing computational power have led to lattice values extremely close to their experimental partners. As the field advances, more improvements can be expected, leading to an even better understanding of QCD.

Although LQCD has indeed much to be proud of, there are still a few issues which need to be ironed out. In this thesis we have discussed how state-of-the-art lattice calculations consistently give low values for the curvature of the nucleon axial form factor. The examination of the hedgehog's form factor may provide some insight into this discrepancy.

It is clear from the results that the model's axial form factor suffers from large finite volume effects. These effects were shown to come from the pion field which was unable to die out by the time it reached the lattice boundary in the smaller volumes. This in turn arose from our periodic boundary condition requiring that the gradient be zero at the lattice value. The finite volume effects on the axial form factor also led to a variation of the axial radius with volume at small pion mass.

These displays of finite volume dependence provide tantalising suggestions that if the lattice size used in the calculation were larger, the values produced by the lattice would be much closer to the empirical values. This further emphasises the point of [TALY05] that the rule of thumb,

$$m_\pi L \gg 4$$

should really be [TALY05]:

$$m_\pi (L - 2R) \gg 4\,,$$

in order to produce results which resemble nature more closely. However, because the model used remains somewhat removed from the lattice situation,

it is impossible to say with full assurance that the described finite volume effects are indeed the cause of the discrepancy in current lattice calculations.

Another possible reason for the lowering of the axial form factor examined was the pion interaction between neighbouring nucleons. Using pion exchange and conventional lattice boundary conditions provided a scenario much closer to the actual situation on the lattice. However, with corrections being around 10 % for a 2 fm box it was not possible to account for the entire difference between lattice and experimental values.

Although a complete explanation for the lower form factor continues to elude the best efforts, this thesis has produced some reasons which may well make up part of any full solution to the problem. Further work is needed, perhaps using the CBM or some other model to ultimately pin down a complete explanation.

Bibliography

[A+10] Alexandrou et al. Axial Nucleon form factors from lattice QCD. 2010.

[AKL+07] Constantia Alexandrou, Giannis Koutsou, Theodoros Leontiou, John W. Negele, and Antonios Tsapalis. Nucleon and Nucleon to Delta Axial form factors from Lattice QCD. *PoS*, LAT2007:162, 2007.

[Ale09] C. Alexandrou. Baryon structure from Lattice QCD. 2009.

[All05] C. R. Allton. Quenching effects in the hadron spectrum. *Lect. Notes Phys.*, 663:1–16, 2005.

[ARZ07] J. Arrington, C. D. Roberts, and J. M. Zanotti. Nucleon electromagnetic form factors. *J. Phys.*, G34:S23–S52, 2007.

[B+10] J. D. Bratt et al. Nucleon structure from mixed action calculations using 2+1 flavors of asqtad sea and domain wall valence fermions. *Phys. Rev.*, D82:094502, 2010.

[BEM02] Veronique Bernard, Latifa Elouadrhiri, and Ulf. G. Meissner. Axial structure of the nucleon. *J. Phys.*, G28:R1–R35, 2002.

[BS04] Silas R. Beane and Martin J. Savage. Baryon axial charge in a finite volume. *Phys.Rev.*, D70:074029, 2004.

[CJJT74] A. Chodos, R. L. Jaffe, K. Johnson, and Charles B. Thorn. Baryon Structure in the Bag Theory. *Phys. Rev.*, D10:2599, 1974.

[Coh02] Thomas D. Cohen. The extraction of g(A) from finite volume systems: The long and short of it. *Phys. Lett.*, B529:50–56, 2002.

[Col] S. Coleman. Soft pions. In *Erice 1967, School *Ettore Majorana**, New York 1968, 9- 50.

[CT75] Alan Chodos and Charles B. Thorn. Chiral Hedgehogs in the Bag Theory. *Phys. Rev.*, D12:2733, 1975.

[D+04] C. T. H. Davies et al. High-precision lattice QCD confronts experiment. *Phys. Rev. Lett.*, 92:022001, 2004.

[D+08] S. Durr et al. Ab-Initio Determination of Light Hadron Masses. *Science*, 322:1224–1227, 2008.

[DD] Thomas DeGrand and Carleton E. Detar. *Lattice methods for quantum chromodynamics*. New Jersey, USA: World Scientific (2006) 345 p.

[DeT81] Carleton E. DeTar. A QUARK BAG MODEL WITH LOW-ENERGY PION INTERACTIONS. 1. THEORY. *Phys. Rev.*, D24:752, 1981.

[DJJK75] Thomas A. DeGrand, R. L. Jaffe, K. Johnson, and J. E. Kiskis. Masses and Other Parameters of the Light Hadrons. *Phys. Rev.*, D12:2060, 1975.

[DL05] William Detmold and C.J.David Lin. Twist-two matrix elements at finite and infinite volume. *Phys.Rev.*, D71:054510, 2005.

[GMT83] Pierre A. M. Guichon, G. A. Miller, and A. W. Thomas. THE AXIAL FORM-FACTOR OF THE NUCLEON AND THE PION - NUCLEON VERTEX FUNCTION. *Phys. Lett.*, B124:109, 1983.

[Gol61] J. Goldstone. Field Theories with Superconductor Solutions. *Nuovo Cim.*, 19:154–164, 1961.

[Gri] David Griffiths. *Introduction to elementary particles*. Weinheim, Germany: Wiley-VCH (2008) 454 p.

[H+08] Ph. Hagler et al. Nucleon Generalized Parton Distributions from Full Lattice QCD. *Phys. Rev.*, D77:094502, 2008.

[HTY] Nathan Hall, Anthony W. Thomas, and Ross D. Young. Axial form factor of the nucleon in a finite volume. To be published.

[IM75] Takuo Inoue and Toshihide Maskawa. The Bag Theory with Dirichlet Boundary Conditions and Spontaneous Symmetry Breakdown. *Prog. Theor. Phys.*, 54:1833, 1975.

[J+76] P. Joos et al. Determination of the Nucleon Axial Vector Form-Factor from pi Delta Electroproduction Near Threshold. *Phys. Lett.*, B62:230, 1976.

[Jaf] R. L. Jaffe. THE BAG. Lectures presented at Erice School of Subnuclear Physics, Erice, Sicily, Jul 31 - Aug 10, 1979.

[LDD+94] K. F. Liu, S. J. Dong, Terrence Draper, J. M. Wu, and W. Wilcox. Nucleon axial form-factor from lattice QCD. *Phys. Rev.*, D49:4755–4761, 1994.

[LMR+05] D. B. Leinweber, W. Melnitchouk, D. G. Richards, A. G. Williams, and J. M. Zanotti. Baryon spectroscopy in lattice QCD. *Lect. Notes Phys.*, 663:71–112, 2005.

[LTY05] D. B. Leinweber, A. W. Thomas, and R. D. Young. Hadron structure and QCD: Effective field theory for lattice simulations. *Lect. Notes Phys.*, 663:113–129, 2005.

[MTT81] G. A. Miller, A. W. Thomas, and S. Theberge. PIONIC CORRECTIONS IN THE MIT BAG MODEL. *Comments Nucl. Part. Phys.*, 10:101, 1981.

[Neu04] H. Neuberger. Lattice field theory: Past, present and future. 2004.

[OY08] Shigemi Ohta and Takeshi Yamazaki. Nucleon structure with dynamical (2+1)-flavor domain wall fermions lattice QCD. 2008.

[Pag75] Heinz Pagels. Departures from Chiral Symmetry: A Review. *Phys. Rept.*, 16:219, 1975.

[PS] Michael E. Peskin and Daniel V. Schroeder. *An Introduction to quantum field theory.* Reading, USA: Addison-Wesley (1995) 842 p.

[Rot92] H. J. Rothe. *Lattice gauge theories: An Introduction*, volume 43. 1992.

[RT10] Giancarlo Rossi and Massimo Testa. A 0-dimensional counter-example to rooting? *Phys. Lett.*, B688:248–249, 2010.

[TALY05] A. W. Thomas, J. D. Ashley, D. B. Leinweber, and R. D. Young. Finite volume dependence of hadron properties and lattice QCD. *J. Phys. Conf. Ser.*, 9:321, 2005.

[Tho84] A. W. Thomas. CHIRAL SYMMETRY AND THE BAG MODEL. *Nucl. Phys.*, A416:69–86, 1984.

[TT83] S. Theberge and A. W. Thomas. MAGNETIC MOMENTS OF THE NUCLEON OCTET CALCULATED IN THE CLOUDY BAG MODEL. *Nucl. Phys.*, A393:252, 1983.

[TTM80] S. Theberge, A. W. Thomas, and G. A. Miller. The Cloudy Bag Model. 1. The (3,3) Resonance. *Phys. Rev.*, D22:2838, 1980.

[TTM81] A. W. Thomas, S. Theberge, and G. A. Miller. The Cloudy Bag Model of the Nucleon. *Phys. Rev.*, D24:216, 1981.

[TW] A. W. Thomas and Wolfram Weise. *The Structure of the Nucleon.* Berlin, Germany: Wiley-VCH (2001) 389 p.

[Wit02] H. Wittig. Cost of dynamical quark simulations: O(a) improved Wilson fermions. *Nucl. Phys. Proc. Suppl.*, 106:197–198, 2002.

[Y+08] T. Yamazaki et al. Nucleon axial charge in 2+1 flavor dynamical lattice QCD with domain wall fermions. *Phys. Rev. Lett.*, 100:171602, 2008.

[You] Ross D. Young. Private communication.

[You04] Ross D. Young. *Finite-Range Regularisation of Chiral Effective Field Theory.* PhD thesis, University of Adelaide, 2004.

[YT10] R. D. Young and A. W. Thomas. Octet baryon masses and sigma terms from an SU(3) chiral extrapolation. *Phys. Rev.*, D81:014503, 2010.